Akman et al. BMC Systems Biology 2010, 4:88
http://www.biomedcentral.com/1752-0509/4/88

BMC Systems Biology

RESEARCH ARTICLE Open Access

Robustness from flexibility in the fungal circadian clock

Ozgur E Akman[1,2,3,5], David A Rand[2,3], Paul E Brown[3], Andrew J Millar[1,2,4*]

Abstract

Background: Robustness is a central property of living systems, enabling function to be maintained against environmental perturbations. A key challenge is to identify the structures in biological circuits that confer system-level properties such as robustness. Circadian clocks allow organisms to adapt to the predictable changes of the 24-hour day/night cycle by generating endogenous rhythms that can be entrained to the external cycle. In all organisms, the clock circuits typically comprise multiple interlocked feedback loops controlling the rhythmic expression of key genes. Previously, we showed that such architectures increase the flexibility of the clock's rhythmic behaviour. We now test the relationship between flexibility and robustness, using a mathematical model of the circuit controlling conidiation in the fungus *Neurospora crassa*.

Results: The circuit modelled in this work consists of a central negative feedback loop, in which the *frequency* (*frq*) gene inhibits its transcriptional activator *white collar-1* (*wc-1*), interlocked with a positive feedback loop in which FRQ protein upregulates WC-1 production. Importantly, our model reproduces the observed entrainment of this circuit under light/dark cycles with varying photoperiod and cycle duration. Our simulations show that whilst the level of *frq* mRNA is driven directly by the light input, the falling phase of FRQ protein, a molecular correlate of conidiation, maintains a constant phase that is uncoupled from the times of dawn and dusk. The model predicts the behaviour of mutants that uncouple WC-1 production from FRQ's positive feedback, and shows that the positive loop enhances the buffering of conidiation phase against seasonal photoperiod changes. This property is quantified using Kitano's measure for the overall robustness of a regulated system output. Further analysis demonstrates that this functional robustness is a consequence of the greater evolutionary flexibility conferred on the circuit by the interlocking loop structure.

Conclusions: Our model shows that the behaviour of the fungal clock in light-dark cycles can be accounted for by a transcription-translation feedback model of the central FRQ-WC oscillator. More generally, we provide an example of a biological circuit in which greater flexibility yields improved robustness, while also introducing novel sensitivity analysis techniques applicable to a broader range of cellular oscillators.

Background

A circadian network (or biological clock) confers a competitive advantage to an organism, probably by enabling it to anticipate cyclic changes in the environment. Circadian rhythms with very similar properties are found in almost all organisms, controlling processes from cyanobacterial cell division to human sleep-wake cycles [1]. There is now evidence that these rhythms can be generated by loops of genes and gene products that communicate by positive and negative feedback. Such loops have been experimentally elucidated for a variety of organisms, including the fungus *Neurospora crassa*, the fly *Drosophila melanogaster* and the plant *Arabidopsis thaliana* [2]. Input signals from light and/or temperature alter the level of one or more components of the loops in order to reset the phase of the rhythm [2].

For the circadian clock to provide an adaptive advantage, it is important for it to maintain the appropriate phase relationship relative to dawn and dusk such that rhythmic biological processes occur at the optimal time of the day. The responses of the clock must ensure that this phase relationship changes appropriately when the clock is subject to regular perturbations - such as

* Correspondence: Andrew.Millar@ed.ac.uk
[1]Centre for Systems Biology at Edinburgh, The University of Edinburgh, Edinburgh, UK

seasonal changes in photoperiod and temperature - while being resilient to the more or less random perturbations resulting from evolutionary processes, external environmental fluctuations or due to the stochastic environment of the cell. The existence of these experimentally tractable system outputs and related performance measures, together with increasingly detailed genetic information, complex dynamics and easy manipulation by light and temperature signals means that circadian clocks are good systems for investigating how the structures of signalling networks affect their system-level properties.

In this vein, recent theoretical and experimental work has focused on elucidating the relationships between the multi-loop architectures characteristic of circadian systems, the flexibility of the clock's dynamic behaviour and the robustness of its function in biological timing [3-9]. Flexibility measures how readily the rhythmic profiles of all the molecular clock components can be altered by modifying the biochemical parameters or environmental inputs of the clock circuit [3]. Robustness focuses on how a biological function, such as the phase of a particular clock component, is maintained under varying conditions. The relationship between these two high-level properties is a complex one, depending on the particular properties of the system of interest. Although flexibility may decrease robustness by increasing sensitivity to perturbations, it can also yield greater robustness by enhancing the ability of the network to tune key environmental responses [10]. Studies within specific circadian systems have had success in identifying the components and structures contributing to their robustness [4,6]. In a more general context, Kitano recently proposed a simple, scalar measure of robustness that aimed to facilitate comparisons across widely differing biological systems [11]. Here, we combine these complementary approaches to analyse the fungal circadian clock.

The Neurospora circadian clock

The fungus *Neurospora crassa* has one of the most comprehensively studied and best understood circadian systems [12,13]. *Neurospora* exhibits a 22 hour rhythm in asexual spore formation (conidiation) when grown in constant darkness (DD) as well as circadian rhythms in metabolism, stress response and other physiological processes [14]. The conidiation rhythm can be entrained by both light and temperature cycles, exhibiting either *systematic* or *driven* entrainment depending on the forcing protocol used [15]. In 24 hr light-dark (LD) cycles, the phase of entrainment (judged by the time of conidiation onset) coincides with the middle of the night in both long and short days [16]. The phase of the clock thus varies systematically with photoperiod: both dusk and dawn signals are integrated to set phase rather than phase being determined solely by either signal alone [15]. By contrast, the clock exhibits driven entrainment in symmetric photic T-cycles (LD cycles of different lengths T with 50% of the cycle in light and 50% in dark). Under these conditions, conidiation onset occurs a fixed time ($\approx$ 7 hrs) after dusk irrespective of cycle length [17].

The core multi-loop genetic oscillator believed to underlie many of the observed circadian rhythms in *Neurospora* - including the conidiation rhythm - is formed by the rhythmic gene *frequency (frq)*, and the constitutively expressed genes *white collar-1 (wc-1)* and *white collar-2 (wc-2)* [13]. The protein products of the *white collar* genes, WC-1 and WC-2, comprise the positive elements of a central negative feedback loop. WC-1 and WC-2 form a heterodimeric WHITE COLLAR complex (WCC) which binds to two light-response elements (LREs) in the *frq* promoter, activating transcription of *frq* [18,19]. The protein product of the *frq* gene is the negative element of the loop. Following transcription of *frq*, two isoforms of FRQ protein are expressed and form homodimeric complexes [20,21]. The relative levels of these isoforms changes with temperature as a result of thermosensitive splicing, yielding a bifurcated, temperature-dependent protein pathway [22,23]. When the expression of the FRQ isoforms reaches a certain level, they interact with the WCC to inhibit its activation of *frq* transcription, closing the negative feedback loop [18,24-28]. The inhibition of *frq* transcription appears to be the consequence of FRQ binding to the WCC and clearing it from the nucleus [28]. The FRQ-WCC interaction is mediated by the protein product of an RNA helicase (*frh*) [29].

As well as forming the negative element of the loop, FRQ positively regulates expression of WC-1, giving a positive feedback loop that interlocks with the primary loop [18,30]. In addition to its essential role in the *Neurospora* feedback loops, WC-1 is a blue-light photoreceptor necessary for photoentrainment. Blue light is perceived by a flavin chromophore (FAD) that binds to the LOV domain of WC-1. The corresponding WCC bound to the LREs at the *frq* promoter is a slower migrating complex than that present in the dark. Light appears to reset the clock by causing an increase in the relative concentration of the slower complex [19], resulting in enhanced transcription of *frq* [31].

In constant darkness, *frq* mRNA is at a minimum level early in the subjective night, peaking early in the subjective day. FRQ peaks 4-6 hrs after its transcript, reaching minimum levels approximately 12 hrs later. *wc-1* mRNA is expressed constitutively, with its protein product oscillating roughly in antiphase with FRQ [19,24-26,30]. In constant light, levels of both *frq* mRNA and FRQ are

elevated and arrhythmic, indicating that the central FREQUENCY-WHITE COLLAR (FRQ-WC) clock is not functioning [31,32]. In 24 hr LD cycles, acute light responses give rise to *frq* mRNA profiles that directly reflect the light environment in different photoperiods; by contrast, the FRQ protein profile appears to determine the onset of conidiation [16].

Modelling the clock

The discovery of the molecular machinery underlying the *Neurospora* circadian network has led to the development of a number of mathematical models of the clock [8,33-39]. These have enabled a range of issues to be addressed regarding the functional relationship between the architecture of the clock and the maintenance of circadian function, including the mechanisms underlying the buffering of free-running period and amplitude against seasonal temperature variations and molecular noise. Thus far, the models developed have primarily concentrated on the expression of the core clock genes in free-running conditions (constant darkness), with the effect of light modelled through direct changes to transcription and degradation rates. Such models therefore have limited use in analysing the photoperiodic responses of the clock.

In this work, we present a model based on the core FRQ-WC oscillator that incorporates both the negative *frq* and positive *wc-1* loops, as well as part of the light-signalling pathway. In addition to simulating the behaviour of the clock in constant conditions (DD), we show that this increased level of biological detail enables our model to reproduce the experimentally observed disassociation between light-driven *frq* mRNA and photoperiodic FRQ protein in 24 hr LD cycles, as well as the driven behaviour seen in symmetric LD T-cycles. This suggests that at least some of the entrainment properties of the *Neurospora* clock can be accounted for by a transcription-translation feedback model of the FRQ-WC oscillator. By using our model to simulate the effect of decoupling the positive *wc-1* loop from the negative *frq* loop, we predict that one of the possible benefits conferred by the presence of the positive loop is robustness of entrained phase against seasonal variations in photoperiod. This yields the experimentally testable prediction that decoupling the loops will result in a dusk-driven clock in long days. The decoupling simulations also provide an additional testable prediction regarding the specific dynamical mechanism underlying the loss of free-running rhythmicity observed in experimental *Neurospora* strains lacking the *wc-1* loop.

We also introduce a simple measure of the flexibility of the network based on quantifying how outputs of the entrained clock vary under parameter perturbations achievable by evolutionary processes [3,40]. Using this measure, we demonstrate that the positive loop yields a more flexible clock. This increased flexibility is shown to be primarily characterised by a greater flexibility in entrained phase, leading to the enhanced robustness against photoperiod fluctuations suggested by the phase simulations. Our results thus provide an example of a cellular circuit where improved robustness is linked directly to increased flexibility.

Results

Description of the model

A network representation of our model of the *Neurospora* clock is shown in Figure 1. The model comprises a set of five coupled ordinary integrodifferential equations describing the dynamics of the two core circadian genes *frq* and *wc-1*. It does not include the genes *wc-2* and *frh* as their protein products form complexes with WC-1 and FRQ respectively and can therefore be combined with these proteins without fundamentally modifying the resulting model. For simplicity, the model in its current form also does not include the light-responsive clock gene *vivid* (*vvd*), a key repressor of light-induced expression controlled by the WCC [41-43], which is believed to sustain a clock that runs during the day [44]. Finally, since we do not consider temperature responses here, we do not differentiate between the two different FRQ isoforms.

Simulations of mRNA and protein profiles

Figures 2 and 3 show simulations of the model in DD and LD conditions respectively. The parameter values used to generate these solutions were obtained by

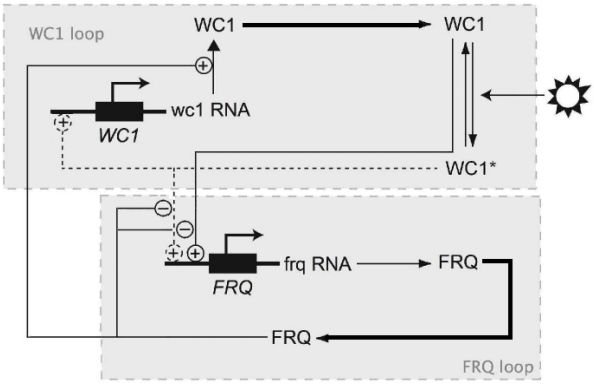

Figure 1 Network diagram for the mathematical model of the Neurospora clock. The model incorporates the core genes *frequency* (*frq*) and *white collar-1* (*wc-1*). The protein product of the *wc-1* gene (WC-1) is the positive element of a central negative feedback loop, while the *frq* protein product (FRQ) is the negative element. FRQ also upregulates the level of WC-1 yielding a positive feedback loop interlocked with the primary one. WC1* represents light-activated WC-1. Thicker lines denote the delay between the translation of a protein and conversion into its active form, modelled using a distributed delay.

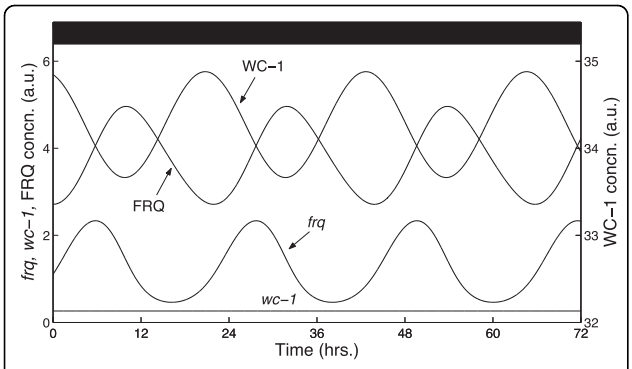

Figure 2 Simulated mRNA and protein profiles in DD. The time series qualitatively match experimental data, yielding: i) an oscillation period close to 22 hrs; ii) constant *wc-1* levels; and iii) a FRQ profile which oscillates in antiphase with WC-1, reaching peak levels shortly after its transcript [19,24-26,30].

minimising a cost function quantifying the goodness-of-fit of the model to experimental time courses [45-48]. This measured how well simulated solutions matched certain key features of the data, such as the free-running period of the clock and the peak and trough phases of the clock components in both free-running and entrained conditions [46]. The DD simulation has a period close to the observed value of 22 hrs, with relative phase relationships also consistent with experimental data: the delay between the peaks of *frq* transcript and FRQ protein is approximately 5 hrs, while FRQ and WC-1 protein oscillate roughly in antiphase.

Furthermore, despite the fact the cost function only assesses goodness-of-fit in simulated 12:12 LD cycles, the optimal solution is a good match to data in long and short days also. As reported experimentally, in all photoperiods for which the clock is stably entrained, *frq* and *wc-1* transcripts exhibit rapid induction at dawn while *frq* expression falls rapidly at dusk, with both transcripts converging to an equilibrium level during the light phase in long days [16]. By contrast, FRQ protein displays markedly smoother changes in expression level, increasing slowly from a minimum level around dawn to a peak level around dusk before degrading back down to its minimum at a roughly constant rate.

Simulations of conidiation onset

Experimental work has suggested a correlation between the FRQ protein profile and the phase of the visible

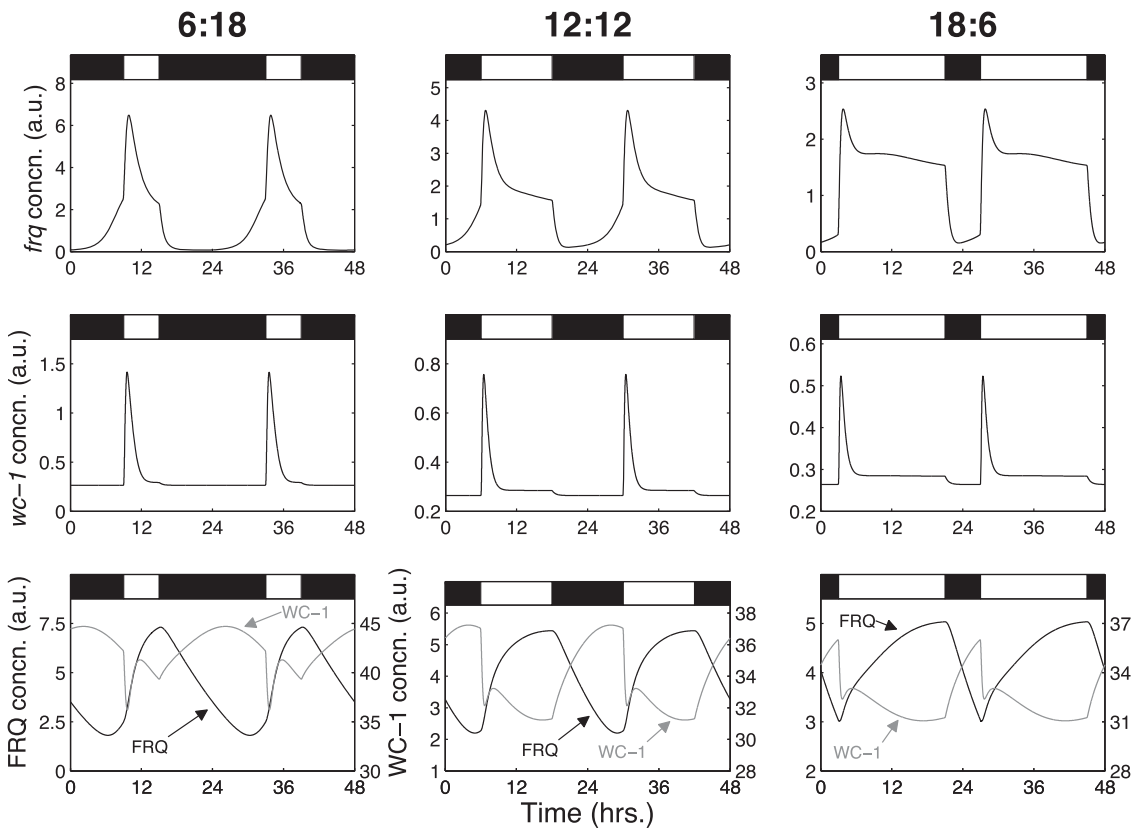

Figure 3 Simulations of the model in different photoperiods. Both *frq* and *wc-1* mRNA exhibit rapid increases in expression at lights-on, while *frq* mRNA also exhibits a rapid decrease in expression at lights-off, consistent with experimental data [16]. The model also reproduces the convergence of *frq* and *wc-1* to equilibrium levels following dawn in longer photoperiods.

rhythm of conidiation onset [15,16]. Specifically, it has been proposed that conidiation phase coincides with a fall in FRQ expression to a point roughly halfway between its maximum and minimum values, possibly as a result of the derepression of a clock output pathway controlling conidia formation. This is based on the observation that in 24 hr LD cycles the decrease in FRQ to the peak-trough midpoint is attained approximately at midnight across photoperiods, coincident with the time at which conidial spores begin to be formed [16].

Figure 4A shows how the simulated phase ϕ_{FRQ} of this molecular conidiation correlate varies with photoperiod. It can be seen that the peak of *frq* mRNA expression is locked to dawn, while the trough is locked to dawn in short days and dusk in all other photoperiods. Conidiation phase ϕ_{FRQ}, however, roughly tracks midnight in agreement with experimental results, even though the cost function used to fit our model to data had no terms involving conidiation time. In our simulations the FRQ-dependent phase of conidiation is thus dissociated from the *frq* mRNA profile which instead directly reflects the light environment, tracking dawn and dusk through its peak and trough phases.

Interestingly, our model also reproduces the driven entrainment observed experimentally in symmetric T-cycles. Figure 5A shows that for T in the range $18 \leq T \leq 24$, FRQ-dependent conidiation onset occurs roughly the same number of hours following dusk irrespective of cycle length; that is, ϕ_{FRQ} tracks dusk. Again, like the variation of ϕ_{FRQ} with photoperiod in 24 hr LD cycles, this is a correctly simulated system-level property that was not a direct target of the cost function. The good fits to phase data can thus be viewed as a validation of our model. For both the T-cycle and photoperiod simulations, we numerically quantified these phase variations by considering the sensitivities of *frq* mRNA and conidiation onset with respect to dawn and dusk, as described below.

Measuring dawn/dusk tracking using dusk sensitivity

The degree to which a circadian phase measure ϕ is sensitive to variations in dawn and dusk is determined by the rate of change $\partial\phi/\partial t_{DUSK}$ of ϕ with respect to the time t_{DUSK} of dusk (here, ϕ can be conidiation onset ϕ_{FRQ} or the times at which *frq* mRNA and FRQ protein are expressed at their minimum and maximum levels). As detailed in section 3 of Additional file 1, this sensitivity measure is bounded between 0 and 1, with a value of 1 indicating a phase that is perfectly locked to dusk and a value of 0 indicating a phase that is perfectly locked to dawn. In light-response plots such as those shown in Figures 4A and 5A, these values correspond to

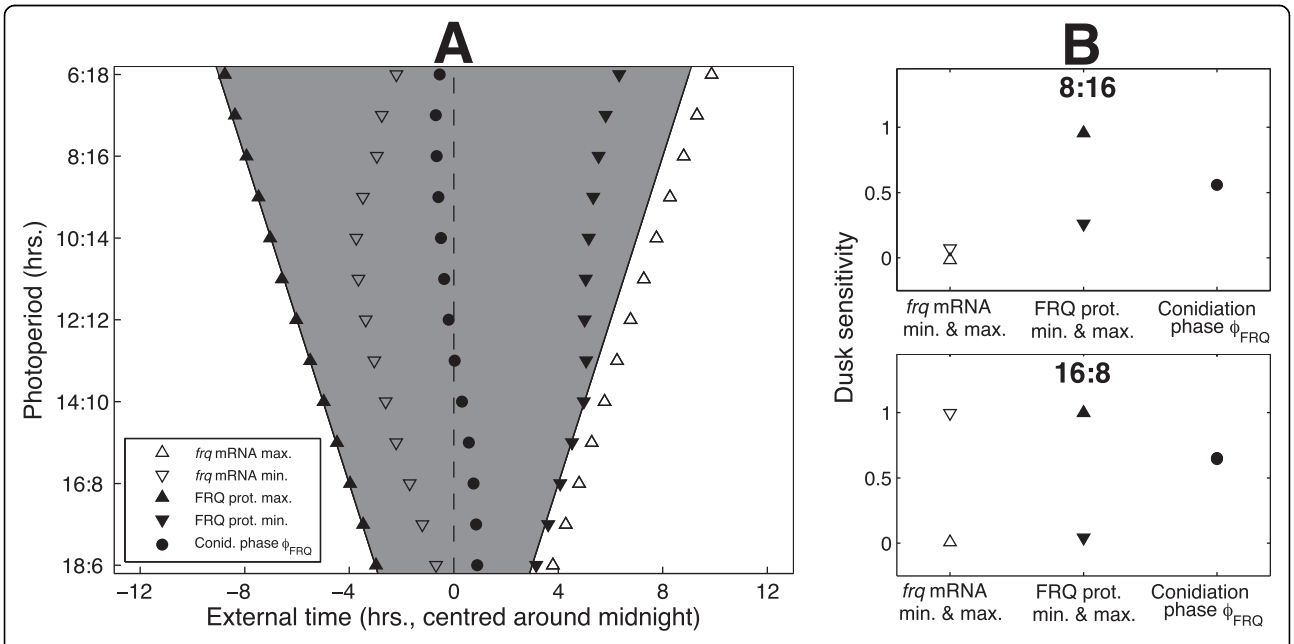

Figure 4 The model reproduces the systematic entrainment observed in LD cycles. **A**. Simulated variation of conidiation onset with photoperiod length. As in [16], conidiation onset was identified with the time ϕ_{FRQ} at which FRQ has decreased to the approximate midpoint of its peak and trough values. Peak and trough times of *frq* mRNA and FRQ protein are also shown. White and grey regions denote light and dark respectively while the dotted line indicates the middle of the night. **B**. Dusk sensitivities $\partial\phi/\partial t_{DUSK}$ of the phase measures plotted in A for short and long days (see Additional file 1, Figure S2A for the sensitivities at intermediate photoperiods). The peak and trough times of *frq* mRNA are locked to either dusk ($\partial\phi/\partial t_{DUSK} = 1$) or dawn ($\partial\phi/\partial t_{DUSK} = 0$). By contrast, conidiation onset ϕ_{FRQ} varies systematically with photoperiod ($\partial\phi_{FRQ}/\partial t_{DUSK} \approx 0.5$).

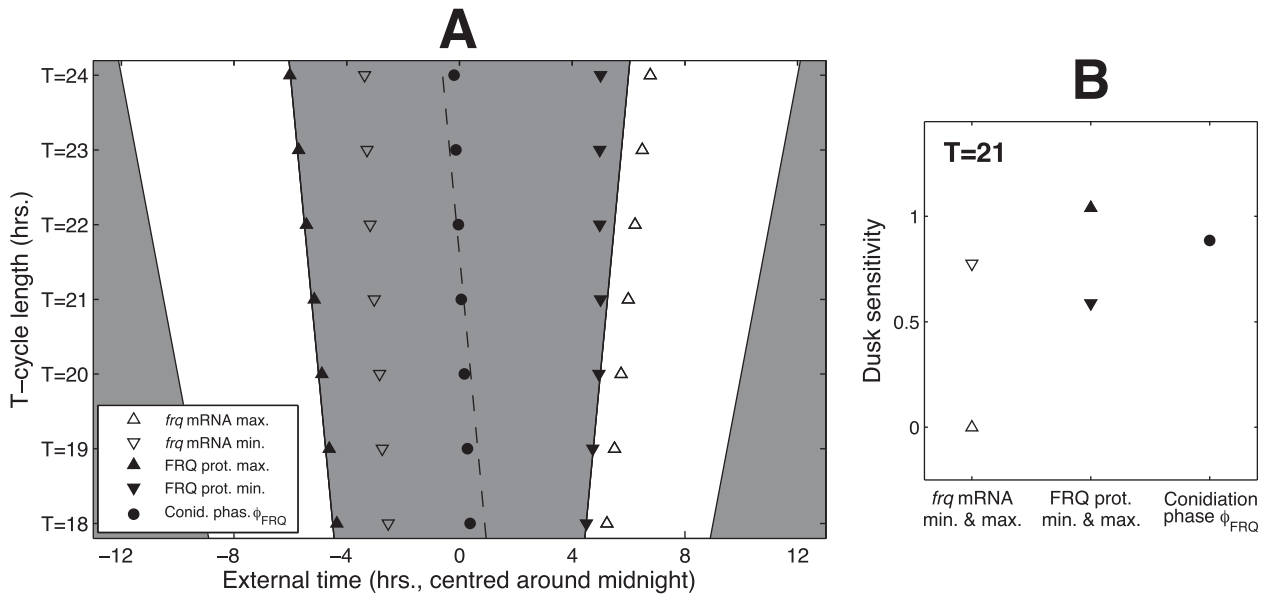

Figure 5 The model reproduces the driven entrainment observed in photic T-cycles. **A**. Simulated variation of conidiation onset with photic T-cycle length. As in Figure 4, conidiation onset was identified with the FRQ falling phase ϕ_{FRQ}. Also plotted are the peak and trough times of *frq* mRNA and FRQ protein. White and grey regions denote light and dark respectively. The dotted line indicates a fixed period of time following dusk. **B**. Dusk sensitivities $\partial\phi/\partial t_{DUSK}$ of the phase measures shown in A for $T = 21$ (see Additional file 1, Figure S3 for the sensitivities over the full range of T-cycle lengths). $\partial\phi_{FRQ}/\partial t_{DUSK}$ is close to 1: conidiation onset therefore tracks dusk.

ϕ lying parallel to the lines indicating the times of dusk and dawn respectively. Intermediate values of $\partial\phi/\partial t_{DUSK}$ correspond to a systematic change in ϕ with photoperiod (ϕ non-parallel to both dusk and dawn). A sensitivity of 0.5 denotes exactly equal responses to dusk and dawn, corresponding to a clock that tracks the middle of the night.

Dusk sensitivities for the model

For 24 hr LD cycles, the disassociation of FRQ-dependent conidiation phase ϕ_{FRQ} from *frq* mRNA expression is shown in terms of the corresponding dusk sensitivity measures in Figure 4B. In short and long days, the phases of peak and trough *frq* expression have dusk sensitivities close to either 0 or 1, indicating locking to dawn and dusk respectively.

Conidiation phase ϕ_{FRQ}, however, has a sensitivity close to 0.5 in both environments, reflecting a near-zero phase change with varying photoperiod. By contrast to the systematic entrainment seen in 24 hr LD cycles, the driven behaviour of ϕ_{FRQ} in symmetric T-cycles is quantified by a $\partial\phi_{FRQ}/\partial t_{DUSK}$ value close to 1 at the intermediate value $T = 21$, indicating a dusk-driven system (see Figure 5B).

Quantifying the effects of positive feedback

A recent computational study compared a model of the *Neurospora* clock incorporating only the central negative *frq* loop with models that also incorporated the positive *wc-1* loop [37]. Simulations of these models - which did not explicitly consider light-signalling - suggested that the *wc-1* loop contributes to the robustness of the system by reducing the sensitivity of the free-running period to parameter fluctuations, while allowing significant variations in oscillation amplitude [37]. Experimental work, however, suggests that decoupling the *wc-1* loop from the *frq* loop leads to the loss of the free-running rhythm altogether [49]. Figure S1A of Additional file 1 shows that reducing positive feedback strength in our model leads to the loss of self-sustained oscillations, consistent with the experimental data.

The good fits of our model to entrainment data (Figures 4A and 5A) did, however, suggest investigating how decoupling the *wc-1* loop affects photoperiodicity. Figure 6A shows the variation of ϕ_{FRQ} with photoperiod when the level of positive feedback is reduced to 50% and 1% of its wild-type value. It can be seen that decreasing the coupling strength advances phase across all photoperiods. However, the simulated decoupling mutants show qualitatively different behaviour in short days versus long days. In short days - despite a phase advance - the mutants still exhibit systematic entrainment with dusk sensitivities $\partial\phi_{FRQ}/\partial t_{DUSK}$ close to the wild-type value of 0.5. In long days, by contrast, reducing the feedback strength causes a transition from systematic to dusk-driven entrainment, quantified by an increase in $\partial\phi_{FRQ}/\partial t_{DUSK}$ from 0.5 to 1.

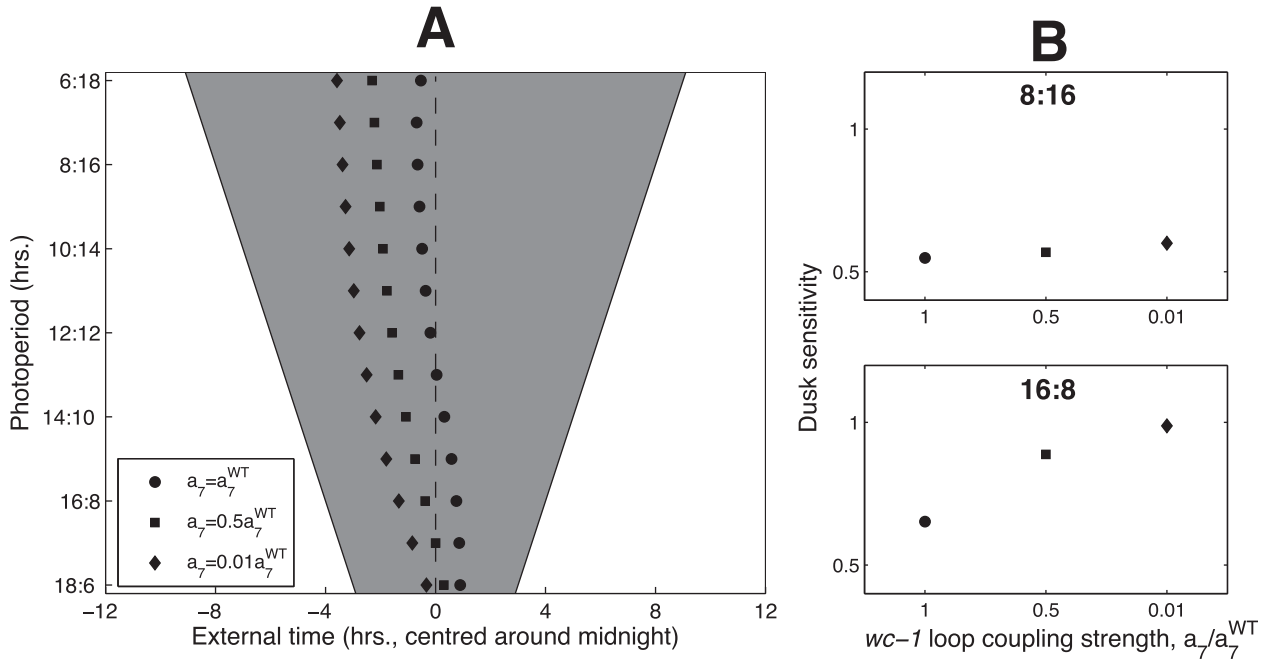

Figure 6 The model predicts that the positive loop promotes systematic entrainment in long days. **A**. The effect of varying the coupling strength of the positive feedback loop on conidiation phase ϕ_{FRQ}. **B**. Conidiation phase dusk sensitivities $\partial\phi_{FRQ}/\partial t_{DUSK}$ computed for short and long days (upper and lower plots respectively). In short days, $\partial\phi_{FRQ}/\partial t_{DUSK}$ remains close to 0.5 as coupling strength is decreased, indicating systematic entrainment. In long days, however, $\partial\phi_{FRQ}/\partial t_{DUSK}$ increases from 0.5 to 1 as positive feedback is abolished, quantifying the transition from an entrained to a (dusk-) driven rhythm that can be seen in A. This transition can be see in greater detail in Additional file 1, Figure S2B which shows the dependence of the sensitivity-photoperiod profile on positive feedback strength.

The wc-1 loop yields phase robustness

The phase and dusk sensitivity plots shown in Figure 6 indicate that the *wc-1* loop may contribute to the robustness of entrained phase against photoperiod variations by enabling systematic entrainment to persist as photoperiod increases. Indeed, systematic entrainment comprises an example of robustness where a property of the whole system can be summarised using a single measure, in line with the general scheme proposed by Kitano [11]. For *Neurospora*, dawn- or dusk-locking (dusk sensitivity equal to 0 or 1) represents the least robust entrainment, which is directly driven by light, while systematic entrainment with a dusk sensitivity of 0.5 is the most robust. Following [11], if we consider variations in photoperiod P over a range $P_1 \le P \le P_2$, then an appropriate quantitative measure of phase robustness $R_{\phi_{FRQ}}$ is

$$R_{\phi_{FRQ}} = \frac{1}{P_2 - P_1}\int_{P_1}^{P_2} D_{\phi_{FRQ}}(P)dP \qquad (1)$$

where $D_{\phi_{FRQ}}(P)$ is an evaluation function bounded between 0 and 1 measuring how the performance of the system varies with P. We chose an evaluation function for which $D_{\phi_{FRQ}}(P_0) = 0$ denotes a clock that is locally driven (i.e. that remains dusk-or dawn-driven for small variations of P around P_0) and $D_{\phi_{FRQ}}(P_0) = 1$ denotes a clock that is locally systematically entrained (i.e. that continues to track the middle of the night under small changes to P). This results in a minimum phase robustness score $R_{\phi_{FRQ}} = 0$ corresponding to a clock that remains locked to either dawn or dusk as P varies over the entire range $P_1 \le P \le P_2$ (global driven entrainment) and a maximum robustness score $R_{\phi_{FRQ}} = 1$ corresponding to a clock that exhibits a systematic variation of phase across the range (global systematic entrainment). The definition of robustness used here is therefore in the sense of maintaining circadian function as parameters are varied, rather than preserving the molecular dynamics of the unperturbed system [11]. The form of the evaluation function used is given in section 4 of Additional file 1.

The robustness index defined in (1) can be used to quantify the effect of decoupling the positive *wc-1* loop from the negative *frq* loop. The ratio of the $R_{\phi_{FRQ}}$ value for a system with modified coupling to that of the WT yields a measure of relative robustness: a score greater than 1 implies a clock that is more robust than the WT; a score less than 1 a less robust network (see Additional file 1, section 4 for details). Figure 7A shows that

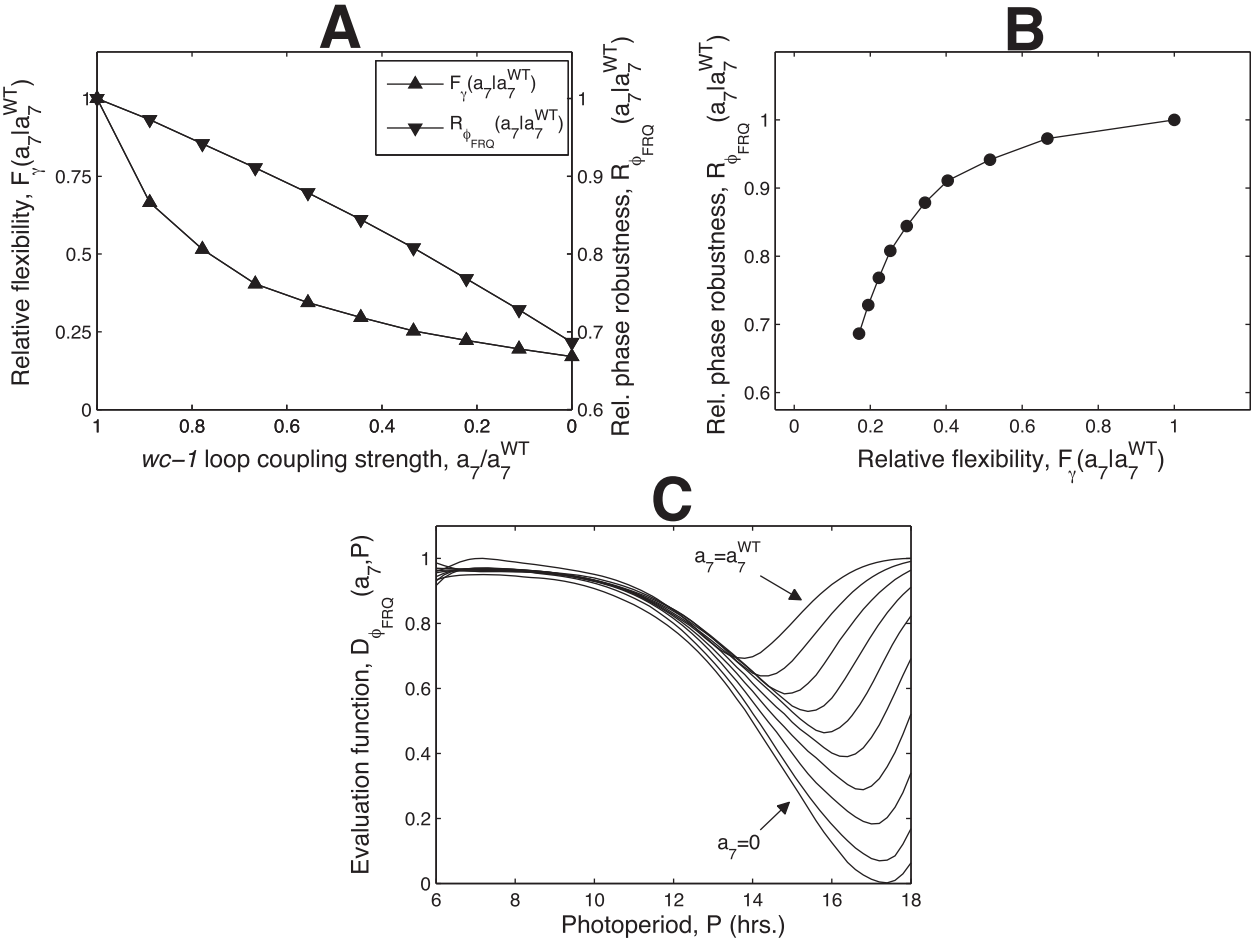

Figure 7 Robustness from flexibility in the Neurospora clock. **A**. Variations in the relative flexibility and robustness of FRQ-dependent conidiation phase with *wc-1* loop coupling strength a_7. Both measures decreases monotonically as the *wc-1* loop is progressively decoupled from the negative *frq* loop. **B**. Relative flexibility and phase robustness are positively correlated, suggesting that one of the benefits of the increased flexibility conferred by the *wc-1* loop is greater phase robustness against photoperiod changes. **C**. Dependence on a_7 of the evaluation function $D_{\phi_{FRQ}}(a_7, P)$ used to compute the relative robustness measure $R_{\phi_{FRQ}}(a_7 \mid a_7^{WT})$ plotted in A. $D_{\phi_{FRQ}}$ measures the extent to which entrained phase varies locally with photoperiod P : driven and systematic entrainment are quantified by $D_{\phi_{FRQ}}$ values of 0 and 1 respectively. In long days, $D_{\phi_{FRQ}}$ decreases to 0 as a_7 is reduced, causing the observed decrease in $R_{\phi_{FRQ}}$.

decoupling the *wc-1* loop reduces the relative robustness of the modified system, as quantified by a significant decrease in the measure from 1. The corresponding changes to the evaluation function are plotted in Figure 7C. It can be seen that while the function remains close to 1 in short days, its value in long days decreases to 0 as positive feedback is removed, reflecting the transition from systematic to dusk-driven entrainment plotted in Figure 6. In this case, therefore, the overall reduction in robustness is largely attributable to the small values of the evaluation function observed for longer photoperiods.

Clock flexibility is increased by the wc-1 loop

The analysis above suggests that the decrease in the robustness of FRQ-dependent entrained phase ϕ_{FRQ} observed on decoupling the *wc-1* loop is related to a loss of flexibility, since for the decoupled system, ϕ_{FRQ} no longer responds to dawn changes in long days. Here we confirm this hypothesis. We demonstrate that reducing the coupling strength causes a reduction in the flexibility of the outputs of the clock, where by output is taken to mean any measure of circadian behaviour that can be computed from the limit cycle attractor of the entrained system (i.e. from the periodic mRNA and protein time series).

In the following, clock flexibility is quantified using a measure based on the formalism established by Rand et al [3,40]. This considers the linearisation of the map between variations in the parameters k of the model and the resulting changes to the entrained limit cycle γ. Parameter variations δk in this scheme are vector changes, in which several parameters can be varied

simultaneously, not just one-at-a time. The corresponding limit cycle changes $\delta\gamma$ are variations in the infinite-dimensional vector obtained by concatenating the periodic time series of each clock component. $\delta\gamma$ thus represents changes to the full state-space representation of the limit cycle [3,40]. As described further in section 5 of Additional file 1, it follows that the singular values of the linearised map between δk and $\delta\gamma$ yield a quantitative measure of the extent to which combinations of random parameter perturbations - which can be considered as representing evolutionary processes - are capable of tuning the outputs of the clock. Geometrically, this map transforms the ball of all possible bounded parameter perturbations into an ellipsoid of output variations. The left singular vectors of the map are the principal axes u_i of this ellipse while the corresponding singular values σ_i (ordered so that $\sigma_i \geq \sigma_{i+1}$) determine the extent of the ellipse along these axes. The right singular vectors v_i are the directions in parameter space that map directly onto these axes.

Within this framework, the clock is flexible if significant changes to its outputs can be obtained with relatively modest parameter changes, as measured by the singular values σ_i. In particular, the sum of the singular values provides a simple flexibility measure, with large values indicating a greater relative change in the outputs for parameter perturbations of a fixed size. It should be noted that this sum is in effect a measure of global sensitivity, in the sense that it considers combined parameter changes, rather than changes to single parameters alone, and the effect of these on the whole periodic solution, not just a single output variable [50]. It follows that the change in flexibility resulting from a change in *wc-1* loop coupling strength can be measured using the ratio of this sum in the modified network to that in the WT (see section 5 of Additional file 1 for details). Values of this relative flexibility index greater than 1 indicate a system that is more flexible than the WT; values less than 1 a less flexible clock. The variation of relative flexibility with coupling strength is plotted in Figure 7A. The corresponding normalised singular value spectra are plotted in Additional file 1, Figure S4. Clearly, flexibility decreases significantly as positive feedback strength is reduced, suggesting that the *wc-1* loop does indeed confer greater flexibility on the network.

It can also be seen in Additional file 1, Figure S4 that for each coupling strength simulated, the dominant singular value σ_1 is larger than the remaining singular values by at least an order of magnitude. This implies that the flexibility of the limit cycle is mainly in the direction of the first principal component vector u_1; that is, the width of the ellipsoid of output perturbations in the direction of the longest principal axis is significantly greater than its width along the remaining axes. The loss of flexibility observed on reducing positive feedback is therefore mainly a consequence of the output ellipsoid contracting along this axis (accompanied by a roughly proportional contraction along the others). We next determined what particular dynamical behaviour this overall lower flexibility reflected, in order to test whether the observed inflexibility of ϕ_{FRQ} was the major change, or one of many effects.

The wc-1 loop primarily affects the flexibility of FRQ protein phase

For a number of weakly forced circadian models, the first principal component has been found to be approximately proportional to the time derivative of the limit cycle [3,40]. This finding implies that perturbations in the direction of the first principal component result in a uniform phase change: that is, all components of the limit cycle are shifted along the time axis by the same amount with no change in amplitude. As described in section 6 of Additional file 1, this can be seen by approximating the perturbed limit cycle as a combination of phase and relative amplitude changes. In the case where the first principal component is approximately proportional to the derivative of the cycle, this yields a zero change in relative amplitude together with a uniform change in phase.

Figure 8A plots the changes in phase and relative amplitude resulting from a perturbation of the WT solution along its first principal component u_1, obtained through a parameter variation in the direction of the corresponding right singular vector v_1. Clearly, FRQ protein undergoes a significantly greater change in phase than *frq* and *wc-1* mRNA. Also, as can be seen in Figure 8B, the large variation in FRQ phase results in a correspondingly large shift of conidiation phase ϕ_{FRQ}. The analysis also implies a non-uniform shift in amplitude, with *wc-1* mRNA exhibiting a greater change compared to *frq* mRNA and FRQ protein (see Figure 8A). These phase/amplitude sensitivity calculations are confirmed by Additional file 1, Figure S5 which plots the corresponding changes to the mRNA and protein time series.

In summary, the results presented here suggest that the increased global flexibility conferred by the *wc-1* loop is primarily an increased flexibility in conidiation phase ϕ_{FRQ}, a particular circadian output which is a direct function of the FRQ protein dynamics. Decoupling the positive *wc-1* loop from the central negative *frq* loop hence yields a circuit for which shifts in conidiation phase of a given size will require relatively larger perturbations to the model parameters. This implication is supported by the significant decrease in phase sensitivity observed on reducing the coupling strength plotted in Figure 8B. The phase-amplitude analysis quantifies the reduction in phase flexibility with positive

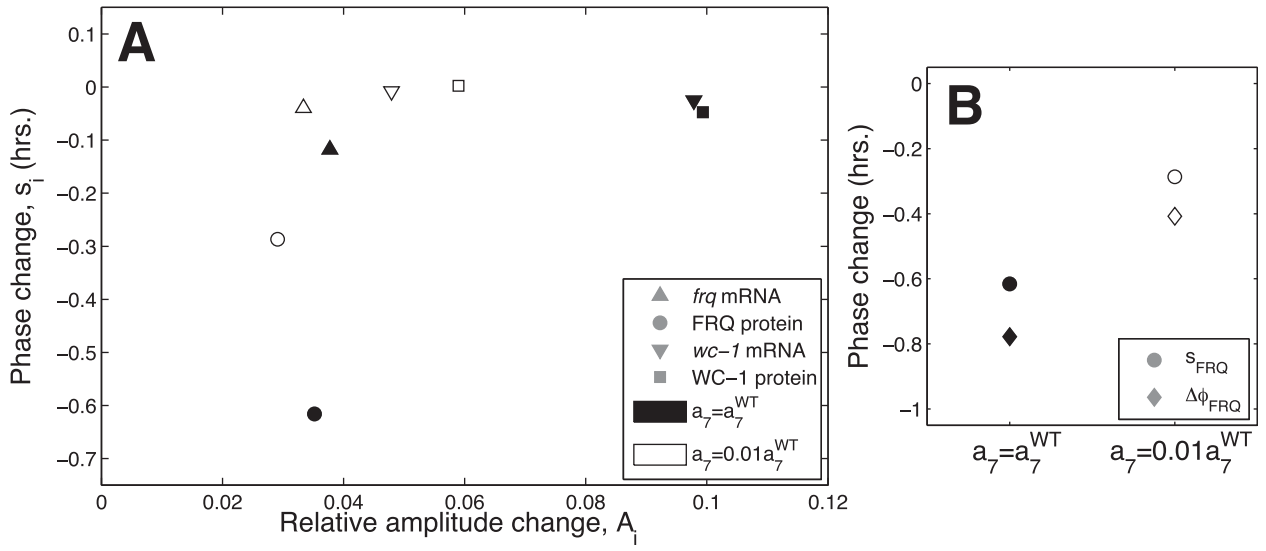

Figure 8 Phase and amplitude sensitivities of the entrained system. **A**. Phase and relative amplitude changes resulting from perturbations of the entrained clock in its maximally flexible direction. Solid and open symbols denote WT and 1% *wc-1* loop coupling respectively. Perturbed solutions were computed for proportional parameter increases of 2%. Note that the reduction in *wc-1* loop coupling strength causes the variation in FRQ protein phase to decrease significantly. **B**. Comparisons of the FRQ phase changes s_{FRQ} for WT and 1% loop coupling with the corresponding changes $\Delta\phi_{FRQ}$ in FRQ-dependent conidiation phase. s_{FRQ} and $\Delta\phi_{FRQ}$ are similar, indicating that the reduced FRQ phase sensitivity also results in reduced conidiation phase sensitivity.

feedback strength that was suggested initially by the simulations of Figure 6. Our simulations and analysis thus predict that one possible phenotypic advantage of the increased global flexibility provided by the *wc-1* loop could be greater robustness of conidiation phase against fluctuations in photoperiod, as summarised in Figure 7B.

Probing the molecular mechanisms underlying phase robustness

The greater robustness conferred by the *wc-1* loop can be understood at the level of molecular dynamics by considering the differential equation describing the dynamics of net FRQ protein, F_T . As demonstrated in section 1 of Additional file 1, the rate of FRQ synthesis is given to a good approximation by the expression below:

$$\dot{F}_T = a_3 M_F - d_2 \frac{P_F}{P_F + b_6} \tag{2}$$

Here, M_F (*t*) and P_F(*t*) are the concentrations of *frq* mRNA and active FRQ, a_3 is FRQ translation rate, d_2 is the maximum rate of FRQ degradation and b_6 is the P_F concentration for which degradation occurs at 50% of its maximum rate. Under LD cycles, *frq* mRNA M_F (*t*) is maintained at low levels during the night, with the exception of the rapid variations that occur around dusk and dawn (see Figure 3). It follows from the form of (2) that if the FRQ degradation rate is strongly saturated (P_F is large compared to b_6), the overall rate of loss of FRQ will be roughly constant during the night. FRQ protein level will hence decrease linearly with time over this period. Furthermore, a constant rate of FRQ loss means that the LD cycle can only affect FRQ levels through the acute light responses of M_F (*t*). Consequently, the rapid induction of *frq* transcription just after dawn will cause the FRQ synthesis rate $\dot{F}_T$ to increase through 0, resulting in a F_T minimum near dawn. Conversely, the rapid decrease in M_F (*t*) just after dusk will cause $\dot{F}_T$ to decrease through 0, producing a F_T maximum near dusk. The combined effects yield a FRQ profile that decays approximately linearly from a peak near dusk to a trough near dawn.

A simple measure of the extent to which FRQ degradation is saturated is provided by the corresponding saturation index $\frac{P_F}{P_F+b_6}$, with values close to 1 indicating strong saturation [51]. The average value D_{SI} of this index during the night then provides a measure of how close the FRQ loss rate is to a constant, with the maximum value of 1 denoting complete saturation between dusk and dawn. It can be seen in Additional file 1, Figure S6 that for all photoperiods, the WT has relatively high D_{SI} values indicating strong saturation of FRQ degradation in the dark. This result is consistent with the FRQ profiles plotted previously in Figure 3 for which FRQ decreases roughly linearly from a dusk-tracking peak to a dawn-tracking trough, resulting in FRQ-dependent conidiation phase ϕ_{FRQ} coinciding with the middle of the night (cf. Figure 4). Figure S6 also

shows that reducing the coupling of FRQ to the *wc-1* loop causes significant decreases in D_{SI} across all photoperiods. The resulting nonlinear dark FRQ profiles move the position of conidiation phase nonuniformly across photoperiods in comparison to the WT, with an enhanced sensitivity to dusk as photoperiod is increased resulting in the lower phase robustness of the decoupling mutants.

The *wc-1* loop thus provides a mechanism for tuning the saturation level of FRQ degradation so as to obtain near-linear dark FRQ profiles for which the peaks and troughs move together with dusk and dawn. This in turn yields a flexible FRQ-dependent conidiation phase ϕ_{FRQ} that responds to both dusk and dawn signals and can therefore track the middle of the night across photoperiods.

Discussion

A model of the Neurospora clock simulating photoentrainment of the FRQ-WC oscillator

Together with *Drosophila melanogaster* and *Arabidopsis thaliana*, *Neurospora crassa* has become a key organism in the computational modelling and analysis of circadian networks. For example, models based on the central negative *frq* loop have been used to investigate the biochemical mechanisms underlying the temperature compensation of the clock [38], together with the effects of molecular noise on the robustness of free-running and entrained rhythms [35]. More complex models incorporating the positive *wc-1* loop have enabled hypotheses to be made regarding the means by which FRQ upregulates WC-1 [37] and inhibits *frq* transcription [39], as well as the possible functional advantages conferred by the positive loop [37] and the parallel pathways comprising the negative loop [8]. These models have proved useful tools in uncovering the design principles of the clock, while also generating a number of important experimental predictions.

Within this framework, we have presented here a mathematical model for the circadian clock of *Neurospora crassa* based on the central FRQ-WC oscillator, incorporating both the *frq* and *wc-1* loops. While previous models of the *Neurospora* clock have modelled the effect of light through direct changes to transcription or degradation rates, we incorporated elements of the light-signalling pathway explicitly in order to be able to quantitatively examine the relationship between network structure and entrained phase. This greater level of biochemical detail enabled us to obtain good fits to experimental data in both free-running and entrained conditions. In particular, we were able to simulate the disassociation between light-driven *frq* mRNA and photoperiodic FRQ protein reported experimentally [16]. While *frq* trough and peak phases are both light-driven in our simulations, FRQ-dependent conidiation phase tracks the middle of the night. The model also reproduces the dusk-driven behaviour observed in symmetric photic T-cycles [15]. In addition, we introduced a novel measure assessing the relative sensitivity of phase to changes in the times of dawn and dusk which provided a quantitative means for distinguishing between the systematic and driven conidiation observed in the photoperiod and T-cycle simulations respectively.

An example of robustness from flexibility

Theoretical and experimental studies have suggested that one of the benefits conferred by multiple feedback loops is increased evolutionary flexibility, with the number of key functionalities of the system that can be tuned independently of one another increasing with the number of loops [3,7,8,40,52]. This greater flexibility can in turn lead to greater robustness of the system against environmental and genetic perturbations [4,6,8,10]. In a previous paper, we gave an example of robustness following from flexibility for the *Neurospora* system using a temperature-dependent variant of the model presented here. In that study, we proposed that the presence of two parallel negative feedback loops with opposing temperature dependence controlling the production of the FRQ isoforms enables low dimensional tuning of the entrainment phase-temperature relationship, facilitating buffering of the clock against seasonal temperature fluctuations [8].

Here, we were interested in investigating how the positive *wc-1* loop affects the clock. Previous computational studies have examined the role of positive feedback on the control of free-running period and amplitude [36,37]. In our model, however, decoupling the *wc-1* loop results in arrhythmicity, in line with experimental observations [49]. More generally, entrained phase rather than free-running period *per se* is expected to have selective value in the natural environment [53,54], thereby identifying phase as a key systems-level output for computational studies [8,55,56]. This led us to examine the effect of decoupling the loop on the robustness of conidiation phase to photoperiod variations. We introduced a robustness index based on the framework proposed by Kitano [11], with maximum robustness being attributed to a system that exhibits systematic entrainment over the full range of photoperiods considered, and minimum robustness to a system that is dusk- or dawn-driven over the same range. Using this measure, we found that removing positive feedback leads to a decrease in phase robustness and that this is a consequence of a transition from systematic to dusk-driven entrainment in long days.

For the next part of the analysis, we introduced a simple scalar measure quantifying the variations in the

outputs of the clock resulting from parameter perturbations mimicking evolutionary processes. This enabled us to demonstrate that the *wc-1* loop enhances the evolutionary flexibility of the clock, consistent with the predictions of previous theoretical studies [3,40]. Using a novel method that is applicable to any entrained biological oscillator, we then computed phase and amplitude sensitivities for perturbations of the clock in its most flexible direction. These sensitivities can be viewed as entrained versions of the period-amplitude sensitivities commonly used to assess the robustness of free-running clocks [36,37,46]. However while the latter are usually computed from scalar perturbations (variations of individual parameters) simulating single mutations, the phase-amplitude sensitivities were obtained by considering vector perturbations that simulate the parameter changes most likely to affect system behaviour under evolutionary changes [3,4,40]. The calculated sensitivities showed that the greater flexibility provided by the *wc-1* loop is predominately manifested as greater flexibility of conidiation phase, a key FRQ-dependent circadian output. Finally, we quantified the molecular basis of the enhanced flexibility - and the resulting robustness of the clock's photoentrainment - demonstrating that the *wc-1* loop provides a low-dimensional mechanism for optimally tuning the extent to which FRQ protein degradation is saturated.

To summarise, our results imply that one of the possible benefits of the increased flexibility conferred by the *wc-1* loop is the persistence of systematic entrainment in long days, contributing to the robustness of the clock with respect to long-term changes in photoperiod. Taken together with previous work, this result could be interpreted as an additional specific example of how increased loop complexity can confer greater flexibility on a cellular circuit, in turn promoting robustness against environmental fluctuations [10].

Predictions and further model development

The work presented here, and previously in [8], predict important roles for the *wc-1* and parallel *frq* loops in maintaining circadian function. This does not necessarily imply that all observed feedback loops in the *Neurospora* circuit need be critical for adaptive clock behaviour. It does, however, demonstrate that detailed models can provide testable predictions regarding the relationship between the constituent loops of the clock and core circadian outputs. The suggestion that decoupling the positive *wc-1* loop from the central feedback loop will abolish systematic entrainment in long days comprises such a prediction and would provide a good test of our model. This prediction could be tested directly by assessing conidiation rhythms in the mutant *frq* strain *frq*-S885/7N, for which WC-1 expression is significantly reduced as a consequence of reduced FRQ phosphorylation [49].

In addition, our model also predicts that the loss of free-running rhythmicity observed in the *frq*-S885/7N strain arises as a consequence of a supercritical Hopf bifurcation (Additional file 1, Figure S1A). The supercritical Hopf bifurcation is one of three typical mechanisms by which periodic oscillations can be destroyed as a system parameter - in this case coupling strength - is altered. For the supercritical Hopf bifurcation of Figure S1A, decreasing the parameter past a certain critical value collapses the DD limit cycle onto an equilibrium point, with the amplitude of oscillations decreasing continuously to zero as this happens. The alternative mechanisms are: i) the destruction of the limit cycle through its collision with an unstable limit cycle generated by a subcritical Hopf bifurcation; and ii) the SNIC (saddle node on invariant circle) bifurcation in which stable and unstable equilibrium points are created simultaneously on the limit cycle [57]. In contrast to the supercritical Hopf, both the subcritical Hopf and SNIC are characterised by a sudden loss of rhythmicity without significant amplitude changes at the bifurcation point [57]. In addition, the SNIC has a distinct experimental signature in which the rhythm freezes at a well-defined phase as the bifurcation is approached.

The particular mechanism that causes arrhythmicity in *frq*-S885/7N could therefore - in principle be ascertained using the strain *frq*-S885/7N;*qa-wc-1* which exhibits QA-induced rhythmic oscillations as a consequence of increased WC-1 expression [49]. Such an experiment would involve observing how the oscillation varied over a range of lower QA concentrations. A progressive fall in rhythmic amplitude as QA concentration is reduced - accompanied by modest changes to both period and phase (cf. Additional file 1, Figure S1B) - would suggest the supercritical Hopf bifurcation predicted by our model. By contrast, a sudden loss of rhythmicity over a narrow range of QA concentrations without a significant amplitude change would be incompatible with our model in its current form. This would instead indicate that either the subcritical Hopf or SNIC bifurcation was responsible for the destruction of the DD limit cycle, with a freezing of phase near the bifurcation point distinguishing the SNIC. In this case, the particular mechanism identified could be used as a target for further model development.

Finally, although our results show that much of the behaviour of the clock in periodic photic cycles can be accurately modelled with the core FRQ-WC oscillator, we note that our model is unable to reproduce some of the responses to shorter light intervals. Specifically, it cannot stably entrain to LD cycles with photoperiods less than 6 hrs, and is also unable to reproduce the

particular form of the type 0 phase response curve (PRC) that has been observed for strong resetting cues in some experiments [41,58]. The expected effect of the VVD protein in modulating the circadian gating of light responses may in part account for these discrepancies. This suggests the inclusion of *vvd* as a suitable next iteration of the model, with PRCs and entrainment to very short days corresponding targets for model validation.

Conclusions

The multi-loop structure of the *Neurospora* clock provides a paradigm example of the extent to which circadian clocks can diverge from the simple delayed negative feedback loop that will reliably oscillate. As experiments lead to the discovery of further clock components and the connections between them in *Neurospora* and other key organisms, mathematical modelling and analysis techniques will become increasingly useful tools in the quantitative analysis of circadian networks. Part of this program will involve the development of ever more detailed models of the complex topologies characteristic of these systems, together with the development of robust algorithms to fit the models to experimental data.

Furthermore, the continuing use of clocks to elucidate the design principles of cellular circuits will require the development of biologically realistic indices of core system-level properties - such as the flexibility and robustness measures presented here -together with analytical tools for their implementation. As an example of this, we anticipate that the global phase-amplitude sensitivity analysis method introduced in this work could prove a useful tool for identifying the particular components of a complex clock network most likely to exhibit functional changes.

Methods

Modelling and parameter fitting

The model equations are given in section 1 of Additional file 1 together with descriptions of their derivation. As in previous clock models, Michaelis-Menten kinetics were used to describe enzyme-mediated degradation of mRNA and active protein while Hill functions were used to model transcriptional activation and inhibition. These equations are taken to abstract sets of more elementary reactions whose biochemical details are unknown [5,7,28,33-36,38,39,46,59-62].

A relative novelty of the model is the way in which the protein pathways have been represented. Many computational models of circadian networks employ sequences of protein modifications (e.g. phosphorylation or nuclear transport) to generate the delays necessary for autonomous oscillations to be produced [61]. We used an alternative, generalised method of representing these delays. This considers the rate at which a protein is converted into its active form to be a weighted sum of the corresponding mRNA levels over the preceding time interval [34,63]. The weights in this sum are the distribution of times for the protein to be modified into its active form; a discrete distribution - concentrated at just one value - corresponds to a single, fixed delay between the translation of a protein and its effect on a downstream gene [64]. Here, we used a continuous distribution (the gamma function) capable of mimicking a variety of biologically plausible delays [65]. A significant advantage of this approach is a marked reduction in complexity as each of the individual parameters representing conversion and degradation of intermediate protein species are replaced by two global parameters governing the form of the gamma function [8,63,65]. For the model considered here, the total number of kinetic parameters was reduced to 33 from a potential maximum value of 45. In addition, the use of a gamma-distributed delay has the advantage of greatly simplifying the analysis of the corresponding set of equations compared to a discrete delay [63,65].

In all, the model comprises five coupled deterministic integrodifferential equations with a total of 36 parameters (the 33 unknown kinetic parameters together with 3 fixed parameters specifying the light input). The large number of unknown model parameters represented a significant challenge in terms of data-fitting, particularly as the free-running and entrained clock have qualitatively different dynamics (while quasi-sinusoidal oscillations are observed in DD, *frq* and *wc-1* mRNA exhibit slow-fast dynamics closer to that of a relaxation oscillator in LD due to acute light responses in these genes). As a consequence of this dual dynamic behaviour - coupled with the significant variability of experimental time courses - we employed a bipartite optimisation method based on minimising a qualitative cost function, rather than attempting to fit directly to data [46].

The cost function we used assessed the goodness-of-fit of the model to both DD and LD experimental time series, based on reproducible circadian measures such as free-running period and the times at which mRNA and protein levels reach their minimum and maximum values [7,8,46,47]. Low cost scores correspond to parameter sets that give a good qualitative match to these target features. The parameter set yielding the smallest cost score was used to generate the simulations of the wild-type clock used in this study. A detailed account of the optimisation technique employed - including a full description of the cost function - is given in section 2 of Additional file 1. The values of the optimal parameter set are listed in Table 1. Simulations of *wc-1* loop uncoupling were obtained by reducing the parameter a_7 controlling the upregulation of WC-1 production by

Table 1 Optimal model parameters

Parameter, k_j	Description	Value
a_1 (h^{-1})	Max. rate: WC-1* upregulated *frq* transcription	8.3450
a_2 (h^{-1})	Max. rate: WC-1 upregulated *frq* transcription	3.7925
a_3 (h^{-1})	FRQ translation rate	0.3154
a_4 (h^{-1})	Basal *wc-1* transcription rate	0.6787
a_5 (h^{-1})	Max. rate: WC-1* upregulated *wc-1* transcription	10.0718
a_6 (h^{-1})	Basal WC-1 translation rate	6.6644
a_7 ($nM^{-1}h^{-1}$)	FRQ upregulated WC-1 translation rate	2.4695
b_1 (nM^{-1})	Michaelis constant: repression of WC-1* upregulated *frq* transcription	4.1472
b_2 (nM)	Michaelis constant: WC-1* upregulated *frq* transcription	0.1560
b_3 (nM^{-1})	Michaelis constant: repression of WC-1 upregulated *frq* transcription	0.7149
b_4 ($nM^{)}$	Michaelis constant: WC-1 upregulated *frq* transcription	2.9415
b_5 (nM)	Michaelis constant: *frq* mRNA degradation	4.1075
b_6 (nM)	Michaelis constant: degradation of active FRQ	0.4715
b_7 (nM)	Michaelis constant: WC-1* upregulated *wc-1* transcription	3.5676
b_8 (nM)	Michaelis constant: *wc-1* mRNA degradation	0.5805
b_9 (nM)	Michaelis constant: degradation of active WC-1	7.0233
b_{10} (nM)	Michaelis constant: degradation of WC-1*	0.8218
d_1 (h^{-1})	Max. rate: *frq* mRNA degradation	7.4608
d_2 (h^{-1})	Max. rate: degradation of active FRQ	0.4405
d_3 (h^{-1})	Max. rate: *wc-1* mRNA degradation	2.1710
d_4 (h^{-1})	Max. rate: degradation of active WC-1	3.0883
d_5 (h^{-1})	Max. rate: degradation of WC-1*	23.3120
f_1 (h^{-1})	Delay parameter: FRQ $\rightarrow$ active FRQ conversion	0.1962
f_2 (h^{-1})	Delay parameter: WC-1 $\rightarrow$ active WC-1 conversion	0.1317
γ_1 (h^{-1})	Loss rate: FRQ $\rightarrow$ active FRQ conversion (deg. rate of intermediates)	0.0422
γ_2 (h^{-1})	Loss rate: WC-1 $\rightarrow$ active WC-1 conversion (deg. rate of intermediates)	0.0244
r_1 (h^{-1})	Rate of active WC-1 $\rightarrow$ WC-1* conversion	5.1759
r_2 (h^{-1})	Rate of WC-1* $\rightarrow$ active WC-1 conversion	5.0326
n	Hill coefficient: WC-1* upregulated *frq* transcription	1.0168
m	Hill coefficient: WC-1 upregulated *frq* transcription	2.8134
k	Hill coefficient: WC-1* upregulated *wc-1* mRNA transcription	1.4135
g	Hill coefficient: repression of WC-1* upregulated *frq* transcription	1.2730
h	Hill coefficient: repression of WC-1 upregulated *frq* transcription	3.6978

Parameter values yielding the optimal value of the cost function used to fit the model to experimental data. WC-1* denotes light-induced active WC-1.

FRQ from its wild-type value ${a_7}^{WT}$ (see Additional file 1, equation (S.4)).

Simulations and software

Solutions of the model were obtained by converting integrodifferential equations into equivalent sets of ordinary differential equations, allowing them to be integrated using standard solvers (see Additional file 1, section 1 for details). Conidiation phase ϕ_{FRQ} was computed as the unique solution of:

$$F_T(\phi_{FRQ}) = (0.5+\alpha)F_T^{PV} + (0.5-\alpha)F_T^{TV};$$
$$F'_T(\phi_{FRQ}) < 0.$$

Here, $F_T(t)$ is the FRQ protein profile, F_T^{PV} and F_T^{TV} represent the peak and trough values of FRQ protein and α is a tuning parameter such that ϕ_{FRQ} coincides with midnight in 12:12 LD cycles. For all simulations presented in this work, α was fixed at the value 0.15.

Model simulations and sensitivity analyses were carried out with custom software developed in MATLAB (Mathworks, Cambridge, UK). Parameter optimisation was implemented by converting numerical routines initially written in MATLAB into C++ and running the code on a task farm computer consisting of 17 × 2.0 GHz 2-way IBM Opteron nodes. All routines used are available by request.

Acknowledgements

The authors would like to thank Sanyi Tang and James Locke for fruitful discussions on clock modelling and parameter optimisation, Isabelle Carré for biological

criticisms and John O'Neill and Laura Dixon for useful comments on the manuscript. The Centre for Systems Biology at Edinburgh is a Centre for Integrative Systems Biology (CISB) funded by BBSRC and EPSRC, reference BB/D019621/1. Funding at Warwick was provided by the BBSRC, EPSRC and EU (BioSim Network Contract No. 005137). This work has made use of the resources provided by the Edinburgh Compute and Data Facility (ECDF) http://www.ecdf.ed.ac.uk/. The ECDF is partially supported by the eDIKT initiative http://www.edikt.org.uk/edikt2/. Additional high-computing facilities were provided by the Centre for Scientific Computing at the University of Warwick http://www.csc.warwick.ac.uk/.

Additional material

Additional file 1: Supplementary Information. This file contains Supplementary Figures S1-S6 together with details of the modelling, parameter optimisation and sensitivity analysis methods used in this work.

Author details
[1]Centre for Systems Biology at Edinburgh, The University of Edinburgh, Edinburgh, UK. [2]Interdisciplinary Programme for Cellular Regulation, University of Warwick, Coventry, UK. [3]Systems Biology Centre, University of Warwick, Coventry, UK. [4]School of Biological Sciences, University of Edinburgh, Edinburgh, UK. [5]School of Engineering, Computing & Mathematics, University of Exeter, Exeter, UK.

Authors' contributions
The model was constructed by OEA, AJM and DAR. Parameter optimisation was carried out by OEA and PEB. Dusk sensitivities and robustness measures were developed by OEA. Flexibility measurements and phase-amplitude analyses were adapted by OEA from analytical techniques proposed by DAR. All simulations and model analyses were carried out by OEA. The paper was written by OEA and AJM. AJM provided biological details, advice and detailed criticism. All authors read and approved the final manuscript.

Received: 27 August 2009 Accepted: 24 June 2010
Published: 24 June 2010

References

1. Dunlap JC, Loros JL, DeCoursey PJ: *Chronobiology: Biological TimeKeeping* Sunderland, MA, Sinauer 2003.
2. Young MW, Kay SA: **Time zones: a comparative genetics of circadian clocks.** *Nat Rev Genet* 2001, **2(9)**:702-15.
3. Rand DA, Shulgin BV, Salazar D, Millar AJ: **Design principles underlying circadian clocks.** *J R Soc Interface* 2004, **1**:119-130.
4. Stelling J, Gilles ED, Doyle FJ: **Robustness properties of circadian clock architectures.** *Proc Natl Acad Sci USA* 2004, **101(36)**:13210-5.
5. Locke JCW, Southern MM, Kozma-Bognar L, Hibberd V, Brown PE, Turner MS, Millar AJ: **Extension of a genetic network model by iterative experimentation and mathematical analysis.** *Mol Syst Biol* 2005, **1**:2005.0013.
6. Wagner A: **Circuit topology and the evolution of robustness in two-gene circadian oscillators.** *Proc Natl Acad Sci USA* 2005, **102(33)**:11775-80.
7. Locke JCW, Kozma-Bognar L, Gould PD, Fehér B, Kevei E, Nagy F, Turner MS, Hall A, Millar AJ: **Experimental validation of a predicted feedback loop in the multi-oscillator clock of Arabidopsis thaliana.** *Mol Syst Biol* 2006, **2**:59.
8. Akman OE, Locke JCW, Tang S, Carré I, Millar AJ, Rand DA: **Isoform switching facilitates period control in the Neurospora crassa circadian clock.** *Mol Syst Biol* 2008, **4**:64.
9. Tsai TY, Choi Y, Ma W, Pomerening JR, Tang C, Ferrell JE Jr: **Robust, tunable biological oscillations from interlinked positive and negative feedback loops.** *Science* 2009, **321(5885)**:126-9.
10. Kitano H: **Biological robustness.** *Nat Rev Genet* 2004, **5(11)**:826-37.
11. Kitano H: **Towards a theory of biological robustness.** *Mol Syst Biol* 2007, **3**:137.
12. Bell-Pedersen D, Crosthwaite SK, Lakin-Thomas PL, Merrow M, Okland M: **The Neurospora circadian clock: simple or complex?** *Philos Trans R Soc Lond B Biol Sci* 2001, **356(1415)**:1697-1709.
13. Loros JJ, Dunlap JC: **Genetic and molecular analysis of circadian rhythms in Neurospora.** *Annu Rev Physiol* 2001, **63**:757-794.
14. Vitalini MW, de Paula RM, Park WD, Bell-Pedersen D: **The rhythms of life: circadian output pathways in Neurospora.** *J Biol Rhythms* 2006, **21(6)**:432-44.
15. Merrow M, Boesl C, Ricken J, Messerschmitt M, Goedel M, Roenneberg T: **Entrainment of the Neurospora circadian clock.** *Chronobiol Int* 2006, **23(1-2)**:71-80.
16. Tan Y, Dragovic Z, Roenneberg T, Merrow M: **Entrainment dissociates transcription and translation of a circadian clock gene in Neurospora.** *Curr Biol* 2004, **14(5)**:433-8.
17. Merrow M, Brunner M, Roenneberg T: **Assignment of circadian function for the Neurospora clock gene frequency.** *Nature* 1999, **399**:584-586.
18. Cheng P, Yang Y, Liu Y: **Interlocked feedback loops contribute to the robustness of the Neurospora circadian clock.** *Proc Natl Acad Sci USA* 2001, **98(13)**:7408-13.
19. Froehlich AC, Liu Y, Loros JJ, Dunlap JC: **White collar-1, a circadian blue light photoreceptor, binding to the frequency promoter.** *Science* 2002, **297(5582)**:815-9.
20. Garceau NY, Liu Y, Loros JJ, Dunlap JC: **Alternative initiation of translation and time-specific phosphorylation yield multiple forms of the essential clock protein FREQUENCY.** *Cell* 1997, **89(3)**:469-76.
21. Cheng P, Yang Y, Heintzen C, Liu Y: **Coiled-coil domain-mediated FRQ-FRQ interaction is essential for its circadian clock function in Neurospora.** *EMBO J* 2001, **20(1-2)**:101-8.
22. Colot HV, Loros JJ, Dunlap JC: **Temperature-modulated alternative splicing and promoter use in the circadian clock gene frequency.** *Mol Biol Cell* 2005, **16(12)**:5563-5571.
23. Diernfellner AC, Schafmeier T, Merrow MW, Brunner M: **Molecular mechanism of temperature sensing by the circadian clock of Neurospora crassa.** *Genes Dev* 2005, **19(17)**:1968-73.
24. Denault DL, Loros JJ, Dunlap JC: **WC-2 mediates WC1-FRQ interaction within the PAS protein-linked circadian feedback loop of Neurospora.** *EMBO J* 2001, **20(1-2)**:109-17.
25. Merrow M, Franchi L, Dragovic Z, Gorl M, Johnson J, Brunner M, Macino G, Roenneberg T: **Circadian regulation of the light input pathway in Neurospora crassa.** *EMBO J* 2001, **20(3)**:307-15.
26. Froehlich AC, Loros JJ, Dunlap JC: **Rhythmic binding of a WHITE COLLAR-containing complex to the frequency promoter is inhibited by FREQUENCY.** *Proc Natl Acad Sci USA* 2003, **100(10)**:5914-9.
27. Schafmeier T, Haase A, Káldi K, Scholz J, Fuchs M, Brunner M: **Transcriptional feedback of Neurospora circadian clock gene by phosphorylation-dependent inactivation of its transcription factor.** *Cell* 2005, **122(2)**:235-46.
28. Hong CI, Ruoff P, Loros JJ, Dunlap JC: **Closing the circadian negative feedback loop: FRQ-dependent clearance of WC-1 from the nucleus.** *Genes Dev* 2008, **22(22)**:3196-3204.
29. Cheng P, He Q, Wang L, Liu Y: **Regulation of the Neurospora circadian clock by an RNA helicase.** *Genes Dev* 2005, **19(2)**:234-41.
30. Lee K, Loros JJ, Dunlap JC: **Interconnected feedback loops in the Neurospora circadian system.** *Science* 2000, **289(5476)**:107-10.
31. Crosthwaite SK, Loros JJ, Dunlap JC: **Light-induced resetting of a circadian clock is mediated by a rapid increase in frequency transcript.** *Cell* 1995, **81(7)**:1003-12.
32. Collett MA, Garceau N, Dunlap JC, Loros JJ: **Light and clock expression of the Neurospora clock gene frequency is differentially driven by but dependent on WHITE-COLLAR-2.** *Genetics* 2002, **160**:149-58.
33. Leloup JC, Gonze D, Goldbeter A: **Limit cycle models for circadian rhythms based on transcriptional regulation in Drosophila and Neurospora.** *J Biol Rhythms* 1999, **14(6)**:433-448.

34. Smolen P, Baxter DA, Byrne JH: **Modeling circadian oscillations with interlocking positive and negative feedback loops.** *J Neurosci* 2001, **21(17)**:6644-56.
35. Gonze D, Halloy J, Goldbeter A: **Robustness of circadian rhythms with respect to molecular noise.** *Proc Natl Acad Sci USA* 2002, **99(2)**:673-8.
36. Smolen P, Baxter DA, Byrne JH: **Reduced models of the circadian oscillators in Neurospora crassa and Drosophila melanogaster illustrate mechanistic similarities.** *OMICS* 2003, **7(4)**:337-54.
37. Francois P: **A model for the Neurospora circadian clock.** *Biophys J* 2005, **88(4)**:2369-2383.
38. Ruoff P, Loros JJ, Dunlap JC: **The relationship between FRQ-protein stability and temperature compensation in the Neurospora circadian clock.** *Proc Natl Acad Sci USA* 2005, **102(49)**:17681-6.
39. Hong CI, Jolma IW, Loros JJ, Dunlap JC, Ruoff P: **Simulating dark expressions and interactions of frq and wc-1 in the Neurospora circadian clock.** *Biophys J* 2008, **94(4)**:1221-32.
40. Rand DA, Shulgin BV, Salazar JD, Millar AJ: **Uncovering the design principles of circadian clocks: mathematical analysis of flexibility and evolutionary goals.** *J Theor Biol* 2006, **238(3)**:616-635.
41. Heintzen C, Loros JJ, Dunlap JC: **The PAS protein VIVID defines a clock-associated feedback loop that represses light input, modulates gating, and regulates clock resetting.** *Cell* 2001, **104(3)**:453-64.
42. Shrode LB, Lewis ZA, White LD, Bell-Pedersen D, Ebbole DJ: **vvd is required for light adaptation of conidiation-specific genes of Neurospora crassa, but not circadian conidiation.** *Fungal Genet Biol* 2001, **32(3)**:169-181.
43. Schwerdtfeger C, Linden H: **VIVID is a flavoprotein and serves as a fungal blue light photoreceptor for photoadaptation.** *EMBO J* 2003, **22(18)**:4846-4855.
44. Elvin M, Loros JJ, Dunlap JC, Heintzen HC: **The PAS/LOV protein VIVID supports a rapidly dampened daytime oscillator that facilitates entrainment of the Neurospora circadian clock.** *Genes Dev* 2005, **19(21)**:2593-605.
45. Brown KS, Sethna JP: **Statistical mechanical approaches to models with many poorly known parameters.** *Phys Rev E* 2003, **68**:021904.
46. Locke JCW, Millar AJ, Turner MS: **Modelling genetic networks with noisy and varied experimental data: the circadian clock in Arabidopsis thaliana.** *J Theor Biol* 2005, **234(3)**:383-93.
47. Zeilinger MN, Farré EM, Taylor SR, Kay SA, Doyle FJ III: **A novel computational model of the circadian clock in Arabidopsis that incorporates PRR7 and PRR9.** *Mol Syst Biol* 2005, **2**:58.
48. Gutenkunst RN, Waterfall JJ, Casey FP, Brown K, Myers CR, Sethna JP: **Universally sloppy parameter sensitivities in systems biology models.** *PLoS Comput Biol* 2007, **3(10)**:1871-78.
49. Schafmeier T, Káldi K, Diernfellner A, Mohr C, Brunner M: **Phosphorylation-dependent maturation of Neurospora circadian clock protein from a nuclear repressor toward a cytoplasmic activator.** *Cell* 2006, **20(3)**:297-306.
50. Rand DA: **Mapping global sensitivity of cellular network dynamics: sensitivity heat maps and a global summation Law.** *J R Soc Interface* 2008, S59-69.
51. Kurosawa G, Iwasa Y: **Saturation of enzyme kinetics in circadian clock models.** *J Biol Rhythms* 2002, **17(6)**:568-577.
52. DePaula RM, Vitalini MW, Gomer RH, Bell-Pedersen D: **Complexity of the Neurospora crassa circadian clock system: multiple loops and oscillators.** *Cold Spring Harb Symp Quant Biol* 2007, **72**:345-51.
53. Ouyang Y, Andersson CR, Kondo T, Golden SS, Johnson CH: **Resonating circadian clocks enhance fitness in cyanobacteria.** *Proc Natl Acad Sci USA* 1998, **95(15)**:8660-4.
54. Dodd AN, Salathia N, Hall A, Kévei E, Tóth R, Nagy F, Hibberd JM, Millar AJ, Webb AA: **Plant circadian clocks increase photosynthesis, growth, survival, and competitive advantage.** *Science* 2005, **309**:630-3.
55. Bagheri N, Doyle FJ: **Quantitative performance metrics for robustness in circadian rhythms.** *Bioinformatics* 2007, **23(3)**:358-64.
56. Gunawan R, Doyle FJ: **Phase sensitivity analysis of circadian rhythm entrainment.** *J Biol Rhythms* 2007, **22(2)**:180-94.
57. Guckenheimer J, Holmes P: *Nonlinear Oscillations, Dynamical Systems and Bifurcations of Vector Fields* New York, Springer Verlag 1983.
58. Dharmananda S: **Studies of the circadian clock of Neurospora crassa: light-induced phase shifting.** *PhD thesis* University of California, Santa Cruz 1980.
59. Ueda HR, Hagiwara M, Kitano H: **Robust oscillations within the interlocked feedback model of Drosophila circadian rhythm.** *J Theor Biol* 2001, **210(4)**:401-6.
60. Gonze D, Halloy J, Goldbeter A: **Biochemical clocks and molecular noise: theoretical study of robustness Factors.** *J Chem Phys* 2002, **116**:10997-11010.
61. Kurosawa G, Mochizuki A, Iwasa Y: **Comparative study of circadian clock models, in search of processes promoting oscillation.** *J Theor Biol* 2002, **216(2)**:193-208.
62. Leloup JC, Goldbeter A: **Toward a detailed computational model for the mammalian circadian clock.** *Proc Natl Acad Sci USA* 2003, **100(12)**:7051-6.
63. MacDonald N: *Biological Delay Systems: Linear Stability Theory* Cambridge, Cambridge University Press 1989.
64. Sriram K, Gopinathan MS: **A two variable delay model for the circadian rhythm of Neurospora crassa.** *J Theor Biol* 2004, **231**:23-38.
65. Mittler JE, Sulzer B, Neumann A, Perelson AS: **Influence of delayed viral production on viral dynamics in HIV-1 infected patients.** *Math Biosci* 1998, **152(2)**:143-163.

doi:10.1186/1752-0509-4-88
Cite this article as: Akman *et al.*: Robustness from flexibility in the fungal circadian clock. *BMC Systems Biology* 2010 **4**:88.

Supplementary Information for ***Robustness from flexibility in the fungal circadian clock.,*** O.E. Akman et al.

Contents

1 Mathematical modelling

1.1 Model equations

The differential equations used to generate the simulations presented in this study are the following:

$$\dot{M}_F = a_1 \frac{\left(P_W^L\right)^n}{\left(1+\left(\frac{P_F}{b_1}\right)^g\right)\left(\left(P_W^L\right)^n + b_2^n\right)} + a_2 \frac{\left(P_W\right)^m}{\left(1+\left(\frac{P_F}{b_3}\right)^h\right)\left(\left(P_W\right)^m + b_4^m\right)} - d_1 \frac{M_F}{M_F + b_5} \quad \text{(S.1)}$$

$$\dot{P}_F = a_3 \int_{-\infty}^{t} M_F(s)\, g_{f_1}(t-s)\, e^{-\gamma_1(t-s)} ds - d_2 \frac{P_F}{P_F + b_6} \quad \text{(S.2)}$$

$$\dot{M}_W = a_4 + a_5 \frac{\left(P_W^L\right)^k}{\left(P_W^L\right)^k + b_7^k} - d_3 \frac{M_W}{M_W + b_8} \quad \text{(S.3)}$$

$$\dot{P}_W = \int_{-\infty}^{t} M_W(s)\left(a_6 + a_7 P_F(s)\right) g_{f_2}(t-s)\, e^{-\gamma_2(t-s)} ds - d_4 \frac{P_W}{P_W + b_9} - r_1\theta(t) P_W + r_2 P_W^L \quad \text{(S.4)}$$

$$\dot{P}_W^L = r_1\theta(t) P_W - r_2 P_W^L - d_5 \frac{P_W^L}{P_W^L + b_{10}}. \quad \text{(S.5)}$$

Here, the variables M_F and M_W denote the concentrations of *frq* and *wc-1* mRNA respectively. P_W is the concentration of active WC-1 and P_W^L represents the concentration of light-induced active WC-1, termed WC-1*. The variable P_F denotes the level of active FRQ. These concentrations are taken to reflect the number of moles per cell and are reported in arbitrary units (a.u.), due to the fact they are not fitted directly to experimental expression levels [1–4].

The repressive action of FRQ on *frq* transcription occurs through the formation of FRQ:WCC complexes followed by FRQ-mediated clearance of the WCC from the nucleus [4]. This process is therefore modelled using terms based on noncompetitive inhibition (equation (S.1)) [2]. The model also includes the positive feedback loop in which FRQ enhances the accumulation of WC-1 (equation (S.4)). Light acts on the system through a smooth function $\theta(t)$ modelling a T-periodic light-dark cycle which switches rapidly between 0 and a maximum value θ_{amp} equal to 1 at dawn ($t = t_{DAWN}$), and from θ_{amp} back to 0 at dusk ($t = t_{DUSK}$):

$$\theta(t) = \frac{\theta_{amp}}{4}\left(1 + \tanh\left(T\left(\bmod(t,T) - t_{DAWN}\right)\right)\right)\left(1 - \tanh\left(T\left(\bmod(t,T) - t_{DUSK}\right)\right)\right).$$

This term acts in two ways. Firstly, it raises the forward rate of the reaction $P_W \rightleftharpoons P_W^L$ in equations (S.4) and (S.5): this models the rise in the relative concentration of FAD-bound WC-1 in complex with the LREs at the *frq* promoter observed with increasing light levels [5], and the resulting enhanced transcription of *frq* [6, 7]. Through this mechanism, it also increases the transcription rate of *wc-1* through the second term of (S.3), reflecting the loss of *wc-1* light-responses in *wc-1* mutant backgrounds [8].

In equations (S.2) and (S.4), the distribution of times required for FRQ and WC-1 protein to be translated and converted into their active forms (through, for example, phosphorylation or nuclear transport) is assumed to be a gamma function with integer scale parameter f_i:

$$g_{f_i}(t) = f_i^2 t e^{-f_i t}.$$

This distribution, commonly referred to as the Erlang distribution, has mean delay $2/f_i$ - representing the average conversion time - and variance $2/f_i^2$ - representing the mean deviation from the average. The term $e^{-\gamma_i t}$ that post-multiplies the Erlang term in (S.2) and (S.4) corresponds to the loss of protein during this process, with γ_i quantifying the rate of loss [9].

1.2 Model simulations

The integrodifferential equations (S.1)-(S.5) can be converted into a set of ordinary differential equations (ODEs) using the linear chain trick [9]. Introducing the auxiliary variables $\left\{E_1^F, E_2^F\right\}$ and $\left\{E_1^W, E_2^W\right\}$ defined by

$$\begin{aligned} E_j^F(t) &= \frac{a_3}{f_1}\int_{-\infty}^{t} G_{f_1}^{j-1}(t-s)\, e^{-\gamma_1(t-s)} M_F(s)\, ds \\ E_j^W(t) &= \frac{1}{f_2}\int_{-\infty}^{t} G_{f_2}^{j-1}(t-s)\, e^{-\gamma_2(t-s)} \left(a_6 + a_7 P_F(s)\right) M_W(s)\, ds \end{aligned}$$

where

$$G_{f_i}^m(t) = \frac{t^m}{m!} f_i^{m+1} e^{-f_i t}$$

enables the equations to be expressed in the form below:

$$\dot{M}_F = a_1 \frac{\left(P_W^L\right)^n}{\left(1+\left(\frac{P_F}{b_1}\right)^g\right)\left(\left(P_W^L\right)^n + b_2^n\right)} + a_2 \frac{\left(P_W\right)^m}{\left(1+\left(\frac{P_F}{b_3}\right)^h\right)\left(\left(P_W\right)^m + b_4^m\right)} - d_1 \frac{M_F}{M_F + b_5} \quad \text{(S.6)}$$

$$\dot{E}_1^F = a_3 M_F - \left(f_1 + \gamma_1\right) E_1^F \quad \text{(S.7)}$$

$$\dot{E}_2^F = f_1 E_1^F - \left(f_1 + \gamma_1\right) E_2^F \quad \text{(S.8)}$$

$$\dot{P}_F = f_1 E_2^F - d_2 \frac{P_F}{P_F + b_6} \quad \text{(S.9)}$$

$$\dot{M}_W = a_4 + a_5 \frac{\left(P_W^L\right)^k}{\left(P_W^L\right)^k + b_7^k} - d_3 \frac{M_W}{M_W + b_8} \quad \text{(S.10)}$$

$$\dot{E}_1^W = \left(a_6 + a_7 P_F\right) M_W - \left(f_2 + \gamma_2\right) E_1^W \quad \text{(S.11)}$$

$$\dot{E}_2^W = f_2 E_1^W - \left(f_2 + \gamma_2\right) E_2^W \quad \text{(S.12)}$$

$$\dot{P}_W = f_2 E_2^W - d_4 \frac{P_W}{P_W + b_9} - r_1 \theta(t) P_W + r_2 P_W^L \quad \text{(S.13)}$$

$$\dot{P}_W^L = r_1 \theta(t) P_W - r_2 P_W^L - d_5 \frac{P_W^L}{P_W^L + b_{10}}. \quad \text{(S.14)}$$

In this formulation, the delays between the translation of FRQ and WC-1 protein and their conversion into active forms - as described by the integrodifferential equations (S.2) and (S.4) - are generated by chains of linear ODEs involving the auxiliary variables. The latter can therefore be thought of as intermediate protein species (e.g. phosphorylated or nuclear/cytoplasmic forms), with the total amounts of FRQ and WC-1 protein given by $F_T = \sum_{i=1}^{2} E_i^F + P_F$ and $W_T = \sum_{i=1}^{2} E_i^W + P_W + P_W^L$ respectively [2]. In particular, summing equations (S.7)-(S.9) yields the following equation for total FRQ synthesis:

$$\dot{F_T} = a_3 M^F - \gamma_1 \left(E_1^F + E_2^F\right) - d_2 \frac{P_F}{P_F + b_6}. \quad \text{(S.15)}$$

Table 1 of the main paper shows that $\gamma_1 \ll 1$. Consequently, (S.15) is well approximated by equation (2) of the main paper.

2 Parameter optimisation

Parameter values $k = (k_1, \ldots, k_s)$ of the model giving a qualitative match to experimental data were obtained by minimising a cost function $C(k)$ comprising a sum of terms measuring the agreement between the model and certain key reproducible features of the data. Following [10], the weighting of each term in the cost function was chosen to yield an O(1) contribution for an experimentally acceptable error. The terms in the cost function were evaluated by numerically solving equations (S.6)-(S.14) over 300 hrs in a simulated 12:12 light dark (LD) cycle, followed by 300 hrs in simulated constant darkness (DD). In each 300 hr interval, the first 204 hrs were discarded as transients.

2.1 Specification of the cost function

The cost function comprises a sum of nine individual terms, each of which corresponds to a set of target qualitative features:

$$\begin{aligned} C &= C_{\tau_{LD}} + C_{OSC_{LD}} + C_{\phi_{LD}} + C_{ALR_{LD}} + C_{PF_{LD}} + C_{\tau_{DD}} \\ &\quad + C_{OSC_{DD}} + C_{\phi_{DD}} + C_{PF_{DD}}. \end{aligned} \quad \text{(S.16)}$$

Here, we provide a description of each of these terms. Throughout this section, simulated time series of *frq* mRNA, *wc-1* mRNA, FRQ protein and WC-1 protein will be denoted by the variables $y_f(t)$, $y_w(t)$, $y_F(t)$ and $y_W(t)$ respectively. The phases at which these variables reach their peak and trough values will be written as θ_i^P and θ_i^T, with $A_i = y_i\left(\theta_i^P\right) - y_i\left(\theta_i^T\right)$ the corresponding oscillation amplitudes and Δ_i^P the times between successive peaks. The operators $\langle . \rangle_{LD}$ and $\langle . \rangle_{DD}$ calculate the average of their arguments over the last 96 hrs of simulation in LD and DD, while $\sigma(.)_{LD}$ and $\sigma(.)_{DD}$ compute the corresponding standard deviations. $[.]_{DD}^B$ and $[.]_{DD}^E$ return the first and last instances of their arguments over the last 96 hours of simulated DD (so, for example, $\left[\theta_F^T\right]_{DD}^B$ calculates the phase of the first FRQ trough encountered over this interval). Finally, L_0 and L_1 denote the times of dusk and dawn.

The first term $C_{\tau_{LD}}$ in (S.16) measures the difference between the period of the solution generated in LD and the target entrained period of 24 hrs:

$$C_{\tau_{LD}} = \sum_{i=f,w,F} \left\langle \left(\left(24 - \Delta_i^P\right)/0.25 \right)^2 \right\rangle_{LD}.$$

The second term $C_{OSC_{LD}}$ penalises large variations in successive peaks, corresponding to solutions that are not properly entrained. It also penalises solutions with very small ($O(10^{-1})$) oscillation magnitudes, as these are unable to generate the large changes in expression level resulting from the system's acute light-responses:

$$C_{OSC_{LD}} = \sum_{i=f,w,F} \left[\left(\sigma\left(y_i\left(\theta_i^P\right)\right)_{LD} / 0.025 \langle y_i\left(\theta_i^P\right)\rangle_{LD} \right)^2 + \left(1.5/\langle A_i \rangle_{LD}\right)^2 \right].$$

The third term $C_{\phi_{LD}}$ calculates the difference between simulated and target phases in LD. It measures the errors for the peak phases of *frq* and *wc-1* mRNA (target phases: 0.5 hrs after dawn)

together with the trough phase of *frq* mRNA (target phase: 3 hrs after dusk) and the peak and trough phases of FRQ protein (target phases: 2 hrs after dusk and dawn respectively). $C_{\phi_{LD}}$ has the form

$$\begin{aligned} C_{\phi_{LD}} &= F_{\phi_{LD}}\left(\theta_f^P, L_1+0.5, 0.5\right) + F_{\phi_{LD}}\left(\theta_f^T, L_0+3, 1\right) + F_{\phi_{LD}}\left(\theta_F^T, L_1+2, 0.5\right) \\ &\quad + F_{\phi_{LD}}\left(\theta_F^P, L_0+2, 0.5\right) + F_{\phi_{LD}}\left(\theta_w^P, L_1+0.5, 0.5\right), \end{aligned}$$

where:

$$F_{\phi_{LD}}\left(\theta_1, \theta_2, E_\theta\right) = \left\langle \left(\left(\theta_1-\theta_2\right)/E_\theta\right)^2 \right\rangle_{LD} + \sigma_{LD}\left(2\left(\theta_1-\theta_2\right)/E_\theta\right)^2.$$

The fourth term $C_{ALR_{LD}}$ checks that *frq* mRNA exhibits both acute dawn and dusk responses and that *wc-1* mRNA exhibits an acute dawn response, as reported in [7]:

$$\begin{aligned} C_{ALR_{LD}} &= \left\langle \left(\frac{\frac{2}{3}A_f}{y_f\left(\theta_f^P\right) - y_f\left(\theta_f^P-2\right)} \right)^2 \right\rangle_{LD} + \left\langle \left(\frac{\frac{1}{2}A_f}{y_f\left(\theta_f^P\right) - y_f\left(\theta_f^P+2\right)} \right)^2 \right\rangle_{LD} \\ &\quad + \left\langle \left(\frac{\exp\left(\frac{5}{3}\right)}{\exp\left(5\left(y_f\left(L_0-1\right) - y_f\left(L_1+1\right)\right)/A_F\right)} \right)^2 \right\rangle_{LD} \\ &\quad + \left\langle \left(\frac{\frac{9}{10}A_w}{y_w\left(\theta_w^P\right) - y_w\left(\theta_w^P-2\right)} \right)^2 \right\rangle_{LD} + \left\langle \left(\frac{\frac{3}{4}A_w}{y_w\left(\theta_w^P\right) - y_w\left(\theta_w^P+2\right)} \right)^2 \right\rangle_{LD}. \end{aligned}$$

The fifth term $C_{PF_{LD}}$ ensures that: 1) *frq* and *wc-1* mRNA profiles stay close to an equilibrium during the light phase of LD cycles; 2) *wc-1* mRNA returns to a near-baseline level following its acute dawn response; and 3) *frq* mRNA does not converge to an equilibrium during the dark phase. It is given by the expression:

$$\begin{aligned} C_{PF_{LD}} &= \left\langle \left(\frac{10\left(y_f\left(\theta_f^P+2\right) - y_f\left(L_0-1\right)\right)}{A_f} \right)^2 \right\rangle_{LD} + \left\langle \left(\frac{10\left(y_w\left(\theta_w^P+2\right) - y_w\left(L_0-1\right)\right)}{A_w} \right)^2 \right\rangle_{LD} \\ &\quad + \left\langle \left(\frac{10\left(y_w\left(\theta_w^T\right) - y_w\left(L_0\right)\right)}{A_w} \right)^2 \right\rangle_{LD} + \left\langle \left(\frac{\frac{1}{10}A_f}{y_f\left(L_1-1\right) - y_f\left(\theta_f^T\right)} \right)^2 \right\rangle_{LD}. \end{aligned}$$

The sixth term $C_{\tau_{DD}}$ measures the deviation of the simulated free-running period from the target period of 22 hours:

$$C_{\tau_{DD}} = \sum_{i=f,W} \left\langle \left(22-\Delta_i^P\right)^2 \right\rangle_{DD}.$$

The seventh term $C_{OSC_{DD}}$ penalises solutions with small ($O(10^{-1})$) free-running amplitudes, bounding the parameter set away from regions where self-sustained rhythmicity can be lost through a supercritical Hopf bifurcation. It also penalises solutions for which: 1) the level of WC-1 protein is very large compared to the level of FRQ protein (some studies, e.g. [11], suggest a low WC-1:FRQ ratio); and 2) the level of FRQ protein is very large compared to that of *frq* mRNA. The term also checks that the peak values and amplitudes of *frq* mRNA and FRQ protein are larger in LD than

in DD. $C_{OSC_{DD}}$ has the form:

$$C_{OSC_{DD}} = \sum_{i=f,F,W} \left(1.5/\left\langle A_i \right\rangle_{DD}\right)^2 + \left\langle \left(\frac{y_W\left(\theta_W^P\right) - y_F\left(\theta_F^P\right)}{3y_F\left(\theta_F^P\right)} \right)^2 \right\rangle_{DD} + \left\langle \left(\frac{y_F\left(\theta_F^P\right) - y_f\left(\theta_f^P\right)}{3y_f\left(\theta_f^P\right)} \right)^2 \right\rangle_{DD} + \sum_{i=f,F} \left[\left(\left\langle A_i \right\rangle_{DD} / \left\langle A_i \right\rangle_{LD} \right)^4 + \left(\left\langle y_i\left(\theta_i^P\right) \right\rangle_{DD} / \left\langle y_i\left(\theta_i^P\right) \right\rangle_{LD} \right)^4 \right].$$

The eighth term $C_{\phi_{DD}}$ measures phase errors in DD, contributing errors of O(1) to C for solutions where FRQ peaks 5 hours after its transcript and oscillates in antiphase to WC-1:

$$C_{\phi_{DD}} = \left\langle \left(\frac{24\left(\theta_F^P - \theta_f^P\right)}{\Delta_f^P} - 5 \right)^2 \right\rangle_{DD} + \left\langle \left(\frac{24\left(\theta_F^T - \theta_W^P\right)}{\Delta_f^P} \right)^2 \right\rangle_{DD} + \left\langle \left(\frac{24\left(\theta_F^P - \theta_W^T\right)}{\Delta_f^P} \right)^2 \right\rangle_{DD}.$$

The ninth and final term $C_{PF_{DD}}$ penalises DD solutions for which: 1) the amplitude and peak value of WC-1 oscillations increases exponentially (indicating blow-up of the solution in this variable); and 2) the amplitude of *frq* oscillations decreases exponentially (corresponding to the convergence of *frq* to an equilibrium). $C_{PF_{DD}}$ is given by the expression

$$C_{PF_{DD}} = F_{PF_{DD}}\left(\left[A_W\right]_{DD}^B, \left[A_W\right]_{DD}^E, 0, 0.25 \right) + F_{PF_{DD}}\left(\left[A_f\right]_{DD}^E, \left[A_f\right]_{DD}^B, 0, 0.25 \right) + F_{PF_{DD}}\left(\left[y_W\left(\theta_W^P\right)\right]_{DD}^B, \left[y_W\left(\theta_W^P\right)\right]_{DD}^E, \left[y_W\left(\theta_W^T\right)\right]_{DD}^B, 0.25 \right),$$

where:

$$F_{PF_{DD}}\left(V_1, V_2, V_3, E_V\right) = \begin{cases} 0 & ;\ \text{if } \mathrm{V}_1 \geq \mathrm{V}_2 \\ \left(\log\left(E_V\right) / \log\left(\left(V_2 - V_1\right) / \left(V_2 - V_3\right)\right)\right)^2 & ;\ \text{if } \mathrm{V}_1 < \mathrm{V}_2 \end{cases}.$$

Low values of $C_{PF_{DD}}$ favour solutions for which the system exhibits autonomous, bounded oscillations in free-running conditions.

2.2 Description of the optimisation algorithm

To find parameter sets consistent with the target experimental features encoded in the cost function C, we first computed the cost at 50 million quasi-randomly distributed points in the 33-dimensional parameter space of the model. These were generated using a variant of the Sobol algorithm [12] in order to obtain uniform coverage of the space [13]. The points were chosen so that all parameters were bounded between 0 and 10, excluding g, n, h, m, k, f_1, f_2, γ_1, γ_2 and a_4. The Hill coefficients g, n, h, m and k were bounded between 1 and 4 [10]. The upper bound ensured that the search for oscillatory solutions of the free-running system did not arbitrarily increase these parameters and hence bias the resulting solutions towards very high levels of transcription factor/promoter cooperativity. f_1 and f_2 were bounded between 0.1 and 1 so as to keep the mean delays in FRQ and WC-1 production between 2 and 20 hrs. γ_1 and γ_2 were bounded above by $0.05 f_1$ and $0.05 f_2$ respectively in order to exclude solutions with low protein survival rates. Finally, a_4 was bounded below d_3 to ensure that *wc-1* mRNA stabilised at a constant level in DD (cf. equation (S.3)).

The 50 solutions with the lowest cost function scores were then passed to a variant of the simulated annealing algorithm described in [14]. The annealing schedule employed comprised a million random steps with a linear temperature decrease. The starting temperature for each parameter set

was taken to be the mean cost function score of the 50 best solutions [10]. During the annealing process, the parameter bounds on g, n, h, m, k, f_1, f_2, γ_1, γ_2 and a_4 detailed above were preserved. In addition, transcription and translation rates ($a_1 \rightarrow a_7$) were allowed to vary between 0 and 100, all Michaelis-Menten constants ($b_1 \rightarrow b_{10}$) were allowed to vary between 0 and 25 , and all transport and degradation transport rates (r_1, r_2 and $d_1 \rightarrow d_5$) were allowed to vary between 1 and 200. The 45 annealed solutions with the lowest values of C were then selected for further analysis. The mean and standard deviation of the cost for these parameter sets was 110.72 and 90.67 respectively, while the optimal parameter set used to generate the simulations shown in the Results section had a cost value $C = 95.27$. Throughout the random search and annealing procedures the cost function was capped at a maximum value $C_{MAX} = 10^4$. A total of 5 optimisation runs were carried out, of which the first 4 were test-runs used to fine-tune the cost function and optimisation protocols. Final parameter sets were taken from the outputs of the 5th run.

2.3 Comparison of experimental and *in silico* protein degradation rates

Although the parameters in our model of the *Neurospora* clock are unknown, necessitating the use of numerical optimisation methods, the rates at which the proteins comprising the core clock are degraded in DD have been estimated experimentally [1, 4]. Below, we derive approximations to these key rates for the model, allowing us to compare the experimental values against those obtained from the optimisation procedure.

In [1] and [4], net FRQ and WC-1 protein degradation rates d_{FRQ} and d_{WC-1} were computed from experimental time courses, assuming first order decay with negligible synthesis following an LL to DD transfer. Following [1, 4], the dynamics of total FRQ protein over the time interval of interest is approximated by:

$$F_T(t) = F_T(0)\, e^{-d_{FRQ} t}. \tag{S.17}$$

Differentiating (S.17), substituting into (S.15) and setting $t = 0$ yields:

$$d_{FRQ} = \frac{1}{F_T(0)} \left(\gamma_1 \left(E_1^F(0) + E_2^F(0) \right) + d_2 \frac{P_F(0)}{P_F(0) + b_6} \right). \tag{S.18}$$

At $t = 0$, $\dot{E}_2^F, \dot{P}_F \approx 0$. Equations (S.7)-(S.9) can therefore be used to express both $P_F(0)$ and $E_2^F(0)$ in terms of $E_1^F(0)$. Using the fact that $\gamma_1 \ll f_1$ and $f_1 E_1^F(0) \ll d_2$ then leads to the approximation below:

$$d_{FRQ} = \frac{\gamma_1 \left(2 + \frac{\gamma_1}{f_1} \right) + f_1}{2 + \frac{\gamma_1}{f_1} + \frac{b_6 f_1}{d_2}}. \tag{S.19}$$

A similar argument yields the following approximation to the net WC-1 degradation rate:

$$d_{WC-1} = \frac{\gamma_2 \left(2 + \frac{\gamma_2}{f_2} \right) + f_2}{2 + \frac{\gamma_2}{f_2} + \frac{b_9 f_2}{d_4}}. \tag{S.20}$$

For both FRQ and WC-1, the net degradation rate thus depends on both the delay parameter and the loss rate for intermediate protein species, together with the maximum rate of active protein degradation and the corresponding Michaelis constant. This complex dependence of the rates on a combination of kinetic parameters was observed previously in a temperature-dependent version of the model considered here [2]. Substituting the optimised values of these parameters into (S.19)

and (S.20) gives $d_{FRQ} = 0.12$ and $d_{WC-1} = 0.07$. These compare favourably with the experimental values $d_{FRQ} = 0.27$ ([1]) and $d_{WC-1} = 0.02$ ([3]), being well within an order of magnitude with FRQ degraded faster than WC-1. The subset of model parameters controlling the degradation rates thus lie within biologically reasonable bounds, indicating that they have been appropriately constrained by the optimisation protocol.

3 Quantifying the sensitivity of phase to changes in dawn and dusk

For 24 hr LD cycles, the sensitivities of a circadian phase measure ϕ with respect to changes in the times of dawn t_{DAWN} and dusk t_{DUSK} are determined by the corresponding partial derivatives $\partial\phi/\partial t_{DAWN}$ and $\partial\phi/\partial t_{DUSK}$. If t_{DAWN} and t_{DUSK} are changed by amounts Δt_{DAWN} and Δt_{DUSK}, then to lowest order the resulting change $\Delta\phi$ in ϕ is given by the expression below:

$$\Delta\phi = \frac{\partial\phi}{\partial t_{DAWN}}\Delta t_{DAWN} + \frac{\partial\phi}{\partial t_{DUSK}}\Delta t_{DUSK}. \tag{S.21}$$

Assuming the clock is stably entrained, perturbing t_{DAWN} and t_{DUSK} simultaneously by the same amount Δt will result in ϕ changing by Δt also. It therefore follows from (S.21) that $\partial\phi/\partial t_{DAWN}$ and $\partial\phi/\partial t_{DUSK}$ always sum to 1. The comparative size of the derivatives thus indicates the relative response of ϕ to changes in dawn and dusk. In particular, a dawn sensitivity $\partial\phi/\partial t_{DAWN}$ equal to 1 means that the phase is locked to dawn since the resulting change in ϕ will be equal to Δt_{DAWN} (and independent of Δt_{DUSK}). In light response plots such as Figures 4A and 6A of the main paper, this corresponds to the line showing the change in ϕ with photoperiod lying exactly parallel to the line indicating the corresponding change in the time of dawn. A dusk sensitivity $\partial\phi/\partial t_{DUSK}$ of 1 implies that the phase is perfectly locked to dusk; in this case ϕ lies parallel to the line indicating the time of dusk.

Since the value of $\partial\phi/\partial t_{DAWN}$ determines that of $\partial\phi/\partial t_{DUSK}$ and vice versa, only one of these is necessary as a measure of the degree of dawn/dusk dominance. Here, we use the dusk sensitivity $\partial\phi/\partial t_{DUSK}$. Values of $\partial\phi/\partial t_{DUSK}$ close to 0 and 1 represent dawn- and dusk-locking respectively, while intermediate values indicate a systematic change in ϕ with photoperiod (ϕ non-parallel to both dawn and dusk). A value of 0.5 denotes exactly equal dawn and dusk sensitivities. For Figures 4A and 6A where photoperiod is varied through equal and opposite changes to dawn and dusk, this corresponds to a net phase change $\Delta\phi$ of zero. This can be seen by substituting $\partial\phi/\partial t_{DAWN} = \partial\phi/\partial t_{DUSK} = 0.5$ and $\Delta t_{DAWN} = -\Delta t_{DUSK}$ into equation (S.21). A zero phase change for such light-forcing protocols denotes a clock that tracks the middle of the night, modulo a fixed phase shift.

Driven and systematic entrainment can also be quantified using the sensitivity of phase with respect to photoperiod, $\partial\phi/\partial P$. Applying the chain rule and using the relations $t_{DAWN} = -t_{DUSK} = P/2$ and $\partial\phi/\partial t_{DAWN} + \partial\phi/\partial t_{DUSK} = 1$ yields:

$$\frac{\partial\phi}{\partial P} = \frac{1}{2}\left(2\frac{\partial\phi}{\partial t_{DUSK}} - 1\right). \tag{S.22}$$

(S.22) shows that $\partial\phi/\partial P$ is bounded between -0.5 and 0.5, with these values indicating dawn- and dusk-locking respectively. Midnight-tracking corresponds to a $\partial\phi/\partial P$ value of 0, as can be seen by setting $\partial\phi/\partial t_{DUSK} = 0.5$.

For the symmetric T-cycles considered in Figure 5 of the main paper, t_{DAWN} and t_{DUSK} are functions of T, with $t_{DAWN} = -t_{DUSK} = T/4$. Consequently, dawn- and dusk-locking correspond to phase derivatives $d\phi/dT$ equal to 1/4 and -1/4 respectively; a derivative of 0 indicates a system that responds equally to both transitions. In this case, the following linear function of the phase derivative provides a suitable dusk sensitivity index:

$$\frac{\partial \phi}{\partial t_{DUSK}} \stackrel{def}{=} \frac{1}{2}\left(1 - 4\frac{d\phi}{dT}\right).$$

By construction, $\partial\phi/\partial t_{DUSK}$ is bounded between 0 (dawn-locking) and 1 (dusk-locking), with a value of 0.5 characterising a clock that tracks midnight.

It should be noted that the sensitivity measures introduced in this section are unaffected by any parameter transformations that preserve the corresponding phase measures. In particular, they are invariant under parameter changes $k = (k_1, \ldots, k_s) \mapsto Rk = (R_1 k_1, \ldots, R_s k_s)$ that result in the components $\gamma_i(t, k)$ of the periodic solution $\gamma(t, k)$ of the entrained model being rescaled (i.e. for which $\gamma_i(t, Rk) = S_i \gamma_i(t, k)$ with $S_i > 0$)). Thus, although our emphasis in this work was to reproduce key qualitative circadian properties preserved across data sets, the sensitivity results presented here would not be altered by any rescaling of the model time series to match a particular set of experimental expression levels.

4 Measuring the robustness of phase to changes in photoperiod

Given a fixed parameter set $k = (k_1, \ldots, k_s)$, the robustness of phase with respect to changes in photoperiod P over a range $P_1 \leq P \leq P_2$ was measured using the quantity

$$R_{\phi_{FRQ}}(k) = \frac{1}{P_2 - P_1}\int_{P_1}^{P_2} D_{\phi_{FRQ}}(k, P)\, dP, \tag{S.23}$$

where the evaluation function $D_{\phi_{FRQ}}(k, P)$ is defined by:

$$D_{\phi_{FRQ}}(k, P) = 4\left(0.5^2 - \frac{\partial \phi_{FRQ}}{\partial P}(k, P)^2\right). \tag{S.24}$$

Recall from section 3 that the sensitivity of entrained phase to photoperiod $\partial\phi_{FRQ}(k, P)/\partial P$ is bounded between -0.5 and 0.5. A sensitivity of 0.5 indicates a clock that is locally dusk-driven (i.e. is locked to dusk in in an interval around P); -0.5 a clock that is locally dawn-driven; and 0 a system that is locally systematically entrained (tracks midnight in an interval around P). It therefore follows from the form of (S.24) that $0 \leq D_{\phi_{FRQ}}(k, P) \leq 1$, with $D_{\phi_{FRQ}}(k, P) = 0$ and $D_{\phi_{FRQ}}(k, P) = 1$ denoting local driven and systematic entrainment respectively. It follows in turn that $0 \leq R_{\phi_{FRQ}}(k) \leq 1$, with minimum robustness indicating global driven entrainment (dawn- or dusk tracking over the entire interval (P_1, P_2)) and maximum robustness indicating global systematic entrainment (midnight-tracking over (P_1, P_2)).

The measure $R_{\phi_{FRQ}}(k)$ can thus be used to quantify the effect of structural changes to the clock circuitry on the robustness of entrained phase with respect to photoperiod. Let k_{WT} and k represent the parameters of the WT and modified systems respectively. Then the ratio below provides a suitable measure of the change in robustness:

$$R_{\phi_{FRQ}}(k|k_{WT}) = \frac{R_{\phi_{FRQ}}(k)}{R_{\phi_{FRQ}}(k_{WT})}.$$

A $R_{\phi_{FRQ}}(k|k_{WT})$ value greater than 1 implies a clock that is more robust than the WT; a value less than 1 implies a system less robust than the WT.

Here, we were interested in the effect of uncoupling the positive *wc-1* loop from the central *frq* loop. Since the coupling strength is determined by the parameter a_7, the measure

$$R_{\phi_{FRQ}}\left(a_7|a_7^{WT}\right) = \frac{R_{\phi_{FRQ}}(a_7)}{R_{\phi_{FRQ}}\left(a_7^{WT}\right)},$$

quantifies how the robustness of entrained phase against photoperiod fluctuations varies with the strength of positive feedback. (In the above, $R_{\phi_{FRQ}}(a_7)$ denotes phase robustness calculated using (S.23) and (S.24) for a feedback strength a_7, with all other kinetic parameters fixed at their WT values). For all computations reported in this work, we chose minimum and maximum photoperiods of $P_1 = 6$ hrs and $P_2 = 18$ hrs respectively

To conclude this section, we recall from the discussion at the end of section 3 that the sensitivity measure $\partial\phi_{FRQ}(k,P)/\partial P$ is invariant under parameter changes $k \mapsto Rk$ which rescale the limit cycle; that is $\partial\phi_{FRQ}(Rk,P)/\partial P = \partial\phi_{FRQ}(k,P)/\partial P$. It therefore follows that $D_{\phi_{FRQ}}(Rk,P) = D_{\phi_{FRQ}}(k,P)$ and hence $R_{\phi_{FRQ}}(Rk) = R_{\phi_{FRQ}}(k)$ (cf. equations (S.23) and (S.24)). Phase robustness is thus also invariant to amplitude rescaling. In particular, any such rescaling will preserve the observed variation in robustness with positive feedback strength.

5 Quantifying network flexibility

5.1 Measuring the flexibility of circadian outputs

The flexibility measure used in this study is based on analysing the map relating parameter variations to changes in key circadian outputs. Following [15, 16], we consider the effect of varying the parameters $k = (k_1, \ldots, k_s)$ of the model on clock outputs Q_j computable from the periodic solution $\gamma(t,k)$ of the model corresponding to the entrained clock (i.e. the limit cycle attractor of the system). Reasonable outputs Q_j within a circadian context here include quantities such as entrained phase, the phases of the minima and maxima of mRNA and protein profiles, the amplitude of these minima and maxima, and - when considering the global flexibility of the system - the entrained limit cycle γ itself [15, 16]. When the parameters are changed (usually by small amounts) then the variation is denoted by $\delta k = (\delta k_1, \ldots, \delta k_s)$. Each variation of the parameters from k to $k + \delta k$ will cause the limit cycle to vary, and this in turn changes the vector of outputs $Q = (Q_1, \ldots, Q_m)$ by an amount $\delta Q = (\delta Q_j)$. The variation δk is an absolute one in that the size of each change δk_i is independent of the size of k_i. However, since the k_is can vary over more than one order of magnitude (see Table 1 of the main paper), it is more appropriate to consider the proportional variation in k_i given by the quantity $\delta\eta_i = \delta k_i/k_i$ (the $\delta\eta_i$s also have the advantage of being dimensionless). If the scaled variations $\delta\eta_i$ are small, then the map $\delta k \mapsto \delta Q$ relating parameter and output changes can be approximated by its linearisation M, the $m \times s$ matrix whose components are the partial derivatives of the individual outputs with respect to the parameters $M_{ij} = \frac{\partial Q_i}{\partial k_j}(k)$. In terms of the scaled parameter changes $\delta\eta = (\delta\eta_i)$, the change δQ in Q is given by

$$\delta Q = M^* \delta\eta, \tag{S.25}$$

where $M^* = M\Delta_k$ is the product of M with the $s \times s$ diagonal matrix $\Delta_k = diag(k_1, \ldots, k_s)$ (the elements of M^* are thus the scaled partial derivatives, $M^*_{ij} = k_j \frac{\partial Q_i}{\partial k_j}(k)$). The changes to the outputs of the system resulting from small random parameter perturbations can therefore be understood by analysing the form of M^*. An important tool in this analysis is the singular value decomposition (SVD) of M^* [15, 16]. The SVD of M^* is its factorisation into the form

$$M^* = U\Sigma V^T, \tag{S.26}$$

where U is an $m \times s$ column-orthonormal matrix ($U^T U = I_s$), V is an $s \times s$ orthonormal matrix ($V^T V = VV^T = I_s$) and $\Sigma = diag(\sigma_1, \ldots, \sigma_s)$ is an $s \times s$ diagonal matrix. The elements $\sigma_1 \geq \cdots \geq \sigma_s \geq 0$ are the singular values of M^* while the columns u_i of U and v_j of V are the left and right singular vectors of M^* respectively [13].

Following [15,16], we consider the changes to the output vector $\delta Q^{(\ell)}$ arising from variations $\delta\eta_i^{(\ell)}$ ($\ell = 1, 2, \ldots, N$) in the scaled parameters, where the $\delta\eta_i^{(\ell)}$s are taken to be zero-mean independent identically distributed random variables with variance $\left\langle \left(\delta\eta_i^{(\ell)}\right)^2 \right\rangle = r_\eta^2$ (angular brackets here denote the expectation of a random variable). As $N \longrightarrow \infty$, this ensemble can be thought of as the set of all possible parameter fluctuations that can result from stochastic evolutionary processes of a bounded size. Provided that r_η is not too large, (S.25) implies that $\delta Q^{(\ell)}$ is approximated by $M^*\delta\eta^{(\ell)}$. It can then be shown that in the limit $N \longrightarrow \infty$, the principal components of the ensemble $\left\{\delta Q^{(\ell)}\right\}$ are the pairs $\left\{u_i, r_\eta^2\sigma_i^2\right\}$ of M^* [16]. The left singular vectors $\{u_1, \ldots, u_s\}$ of M^* thus provide an orthogonal coordinate system within which the $\delta Q_i^{(\ell)}$s are uncorrelated, with variances equal to $r_\eta^2\sigma_i^2$. Geometrically, the ensemble $\left\{\delta\eta^{(\ell)}\right\}$ can be thought of as a ball of parameter perturbations that are mapped to an ellipsoid of output perturbations $\left\{\delta Q^{(\ell)}\right\}$ by M^*; u_i and $r_\eta\sigma_i$ are then the ith principal axis of the ellipse and the extent of the ellipse along this axis respectively. The singular values σ_i thus quantify the effect of random parameter perturbations on the output Q. Furthermore, a scalar measure of the size of the output variations is provided by the net variance $r_\eta^2 \sum_{i=1}^s \sigma_i^2$ (it is straightforward to show that this is equal to the average of the squared output perturbation size, $\left\langle \left\| \delta Q^{(\ell)} \right\|^2 \right\rangle$). The sum of the singular values $\sum_{i=1}^s \sigma_i^2$ therefore provides a simple measure of the flexibility of Q: the larger this sum, the greater the relative change in Q under random parameter perturbations. In addition, the left singular vectors u_i associated with the largest singular values indicate the most flexible (or evolutionarily accessible) directions in the output space. These are the directions along which relatively large changes in Q can be obtained with comparatively small changes $\delta\eta$ in the parameters. Geometrically, these correspond to the principal axes of the ellipsoid of output perturbations along which it has greatest extent [15, 16]. The corresponding right singular vectors v_i represent the parameter changes that lead to variations along the principal axes of the ellipsoid: i.e. those parameter variations most likely to be achieved by evolutionary processes.

5.2 Calculating the relative flexibility of the clock network

In order to quantify the effect on circadian flexibility of perturbations to the wild-type parameter set k_{WT}, we consider a relative flexibility measure given by the expression below:

$$F_Q(k|k_{WT}) = \frac{\sum_{i=1}^s \sigma_i(k)^2}{\sum_{i=1}^s \sigma_i(k_{WT})^2}.$$

Here, $\sigma_i(k_{WT})$ and $\sigma_i(k)$ are the singular values for the WT and modified system respectively. If $F_Q(k|k_{WT})$ is greater than 1, Q is more flexible in the modified system than in the WT, while if it is less than 1 it is less flexible.

For the *Neurospora* model, we were interested in the effect of reducing the strength of FRQ's positive feedback on WC-1 production. As all circadian outputs of interest can be computed from the limit cycle attractor γ of the entrained system, a suitable global flexibility index for this analysis is provided by:

$$F_\gamma\left(a_7|a_7^{WT}\right) = \frac{\sum_{i=1}^{s}\sigma_i(a_7)^2}{\sum_{i=1}^{s}\sigma_i\left(a_7^{WT}\right)^2}. \tag{S.27}$$

For a given positive feedback strength a_7, $F_\gamma\left(a_7|a_7^{WT}\right)$ compares the variance of the corresponding limit cycle under random parameter perturbations to the variance for WT coupling; values less than 1 indicate a system that is less flexible than the WT.

In (S.27), $\sigma_i(a_7)$ is the ith singular value of the matrix M^* relating parameter perturbations $\delta\eta$ to the corresponding change δQ to the vector of system outputs Q in the case where Q is the entrained limit cycle γ (cf. equation (S.25)). Writing the ith component of $\gamma(t,k)$ as $\gamma_i(t,k)$, Q is therefore the infinite-dimensional vector

$$Q = \left(\gamma_1(0,k),\ldots,\gamma_1(T,k),\gamma_2(0,k),\ldots,\gamma_2(T,k)\ldots,\gamma_4(0,k),\ldots,\gamma_4(T,k)\right)^T, \tag{S.28}$$

where T is the period of the forcing light-dark cycle and $\gamma_1 \longrightarrow \gamma_4$ are *frq* mRNA, *wc-1* mRNA, total FRQ protein and total WC-1 protein concentrations respectively. The matrix $M^* = \left(k_j\frac{\partial\gamma_i}{\partial k_j}(t,k)\right)$ is thus the linearisation of a map from scaled parameter variations $\delta\eta \in \mathbb{R}^s$ to the space of T-periodic, 4-dimensional, smoothly differentiable real-valued functions [15, 16]. Following [15, 16], singular values and vectors were calculated from a finite approximation to M^* obtained by restricting time t to a discrete set of $N \gg 1$ evenly spaced values in the interval $[0,T]$.

Finally, it is straightforward to show that normalising the derivative $\frac{\partial\gamma_i}{\partial k_j}(t,k)$ in M^* by the magnitude of the limit cycle $\|\gamma_i(t,k)\|$ preserves the SVD under the amplitude rescaling parameter transformations discussed in sections 3 and 4.[1] It follows that the corresponding flexibility measure $\hat{F}_\gamma$ is also invariant under any rescaling of this type. We found that the variation of $\hat{F}_\gamma$ with positive feedback strength a_7 is very similar to that observed for the non-normalised measure F_γ. Thus - despite the greater generality of the normalised measure - non-normalised flexibility is plotted in Figure 7 of the main paper for simplicity.

6 Phase and amplitude variations for the entrained limit cycle

The limit cycle $\gamma_i(t,k)$ resulting from a general parameter perturbation $k_0 \mapsto k$ can be approximated by the combination of a phase change $s_i(k)$ and a relative amplitude change $A_i(k)$:

$$\gamma_i(t,k) = (1+A_i(k))\gamma_i(t+s_i(k),k_0). \tag{S.29}$$

[1] Here, $\|.\|$ is the norm induced by the inner product $\langle p(t),q(t)\rangle = \frac{1}{T}\int_0^T p(s)\,q(s)\,ds$, so that $\|p(t)\| = \sqrt{\langle p(t),p(t)\rangle} = \sqrt{\frac{1}{T}\int_0^T p(s)^2\,ds}$.

A perturbation of magnitude α in a particular direction w results, to lowest order, in the phase and amplitude variations

$$s_i(k) = \alpha \frac{\partial s_i}{\partial w}(k_0), \tag{S.30}$$

$$A_i(k) = \alpha \frac{\partial A_i}{\partial w}(k_0), \tag{S.31}$$

where $\partial s_i(k_0)/\partial w$ and $\partial A_i(k_0)/\partial w$ denote the directional derivatives of $A_i(k)$ and $S_i(k)$ along w evaluated at k_0. Here, we derive analytical expressions for these derivatives in terms of the principal components of γ. We also show that in the case when the first principal component u_1 is proportional to the derivative of the limit cycle, that is $u_1 = \beta\dot{\gamma}$, the derivatives along the principal parameter direction v_1 take the values $\partial s_i(k_0)/\partial v_1 = \beta\sigma_1$ and $\partial A_i(k_0)/\partial v_1 = 0$. This implies that $s_i(k) \approx \alpha\beta\sigma_1$ and $A_i(k) \approx 0$, corresponding to a uniform phase change (cf. equations (S.29)-(S.31)).

Write $k_0 = (k_{01}, \ldots, k_{0s})$. Since we consider proportional parameter changes here, $\partial s_i(k_0)/\partial w$ and $\partial A_i(k_0)/\partial w$ are given by the expressions below:

$$\frac{\partial s_i}{\partial w}(k_0) = \left(k_{01}\frac{\partial s_i}{\partial k_1}(k_0), \ldots, k_{0s}\frac{\partial s_i}{\partial k_s}(k_0) \right) \cdot w, \tag{S.32}$$

$$\frac{\partial A_i}{\partial w}(k_0) = \left(k_{01}\frac{\partial A_i}{\partial k_1}(k_0), \ldots, k_{0s}\frac{\partial A_i}{\partial k_s}(k_0) \right) \cdot w. \tag{S.33}$$

Differentiating both sides of (S.29) with respect to k_j implies the following equation for $\partial\gamma_i(t,k_0)/\partial k_j$:

$$\frac{\partial \gamma_i}{\partial k_j}(t,k_0) = \frac{\partial s_i}{\partial k_j}(k_0)\,\dot{\gamma}_i(t,k_0) + \frac{\partial A_i}{\partial k_j}(k_0)\,\gamma_i(t,k_0).$$

Using the identity $\int_0^T \gamma_i(s,k)\,\dot{\gamma}_i(s,k)\,ds = 0$ then yields

$$k_{0j}\frac{\partial s_i}{\partial k_j}(k_0) = \frac{\left\langle k_{0j}\frac{\partial \gamma_i}{\partial k_j}(t,k_0), \dot{\gamma}_i(t,k_0)\right\rangle}{\|\dot{\gamma}_i(t,k_0)\|^2} \tag{S.34}$$

and

$$k_{0j}\frac{\partial A_i}{\partial k_j}(k_0) = \frac{\left\langle k_{0j}\frac{\partial \gamma_i}{\partial k_j}(t,k_0), \gamma_i(t,k_0)\right\rangle}{\|\gamma_i(t,k_0)\|^2}. \tag{S.35}$$

The terms $k_{0j}\partial\gamma_i(t,k_0)/\partial k_j$ in (S.34) and (S.35) are the elements of the matrix M^*. It therefore follows from the SVD expansion (S.26) of M^* that

$$k_{0j}\frac{\partial s_i}{\partial k_j}(t,k_0) = \frac{\sum_{l=1}^{s}\sigma_l v_{jl}\left\langle u_l^i(t,k_0), \dot{\gamma}_i(t,k_0)\right\rangle}{\|\dot{\gamma}_i(t,k_0)\|^2} \tag{S.36}$$

and

$$k_{0j}\frac{\partial A_i}{\partial k_j}(t,k_0) = \frac{\sum_{l=1}^{s}\sigma_l v_{jl}\left\langle u_l^i(t,k_0), \gamma_i(t,k_0)\right\rangle}{\|\gamma_i(t,k_0)\|^2}, \tag{S.37}$$

where v_{jl} is the (j,l)th element of the matrix V and $u_l^i(t,k_0)$ represents the element of the vector u_l occupying the same position as $\gamma_i(t,k_0)$ in the representation of the limit cycle as an infinite-dimensional vector (cf. equation (S.28)). Substituting (S.36) and (S.37) into (S.32) and (S.33)

respectively and using the relation $V^TV = I_s$ leads to the final expressions for $\partial s_i(k_0)/\partial w$ and $\partial A_i(k_0)/\partial w$ below:

$$\frac{\partial s_i}{\partial w}(k_0) = \frac{\sum_{l=1}^{s}(v_l \cdot w)\,\sigma_l \left\langle u_l^i(t,k_0), \dot{\gamma}_i(t,k_0)\right\rangle}{\|\dot{\gamma}_i(t,k_0)\|^2}, \tag{S.38}$$

$$\frac{\partial A_i}{\partial w}(k_0) = \frac{\sum_{l=1}^{s}(v_l \cdot w)\,\sigma_l \left\langle u_l^i(t,k_0), \gamma_i(t,k_0)\right\rangle}{\|\gamma_i(t,k_0)\|^2}. \tag{S.39}$$

The phase derivative is thus obtained by projecting the principal components of the limit cycle onto the derivative of the cycle while the amplitude derivative is obtained by projection onto the cycle itself.

In the case when the first principal component is proportional to the derivative, so that $u_1^i(t,k_0) = \beta\dot{\gamma}_i(t,k_0)$, setting $w = v_1$ in (S.38) and (S.39) implies

$$\frac{\partial s_i}{\partial v_1}(k_0) = \frac{\beta\sigma_1 \left\langle \dot{\gamma}_i(t,k_0), \dot{\gamma}_i(t,k_0)\right\rangle}{\|\dot{\gamma}_i(t,k_0)\|^2} = \beta\sigma_1$$

since $\left\langle \dot{\gamma}_i(t,k_0), \dot{\gamma}_i(t,k_0)\right\rangle = \|\dot{\gamma}_i(t,k_0)\|^2$, and

$$\frac{\partial A_i}{\partial v_1}(k_0) = \frac{\beta\sigma_1 \left\langle \dot{\gamma}_i(t,k_0), \gamma_i(t,k_0)\right\rangle}{\|\gamma_i(t,k_0)\|^2} = 0$$

since $\left\langle \dot{\gamma}_i(t,k_0), \gamma_i(t,k_0)\right\rangle = 0$. The perturbation along v_1 thus results in a uniform phase change, as claimed.

We conclude by remarking that in common with the phase sensitivity and robustness measures discussed in sections 3 and 4, $\partial s_i(k_0)/\partial w$ and $\partial A_i(k_0)/\partial w$ are also invariant under parameter transformations that rescale amplitude, $\gamma_i(t,k_0) \mapsto S_i\gamma_i(t,k_0)$. This is a consequence of the fact that in addition to scaling $\gamma_i(t,k_0)$ (and hence $\dot{\gamma}_i(t,k_0)$) by S_i, such a transformation will scale the elements $u_l^i(t,k_0)$ of U in the factorisation $M^* = U\Sigma V^T$ by S_i also. The invariance of the derivatives then follows directly from the forms of (S.38) and (S.39).

References

[1] Ruoff P, Loros JJ, Dunlap JC: **The relationship between FRQ-protein stability and temperature compensation in the Neurospora circadian clock**. *Proc Natl Acad Sci USA* 2005, **102**(49):17681–6.

[2] Akman OE, Locke JCW, Tang S, Carré I, Millar AJ, Rand DA: **Isoform switching facilitates period control in the Neurospora crassa circadian clock.** *Mol Sys Biol* 2008, **4:64**.

[3] Hong CI, Jolma IW, Loros JJ, Dunlap JC, Ruoff P: **Simulating dark expressions and interactions of frq and wc-1 in the Neurospora circadian clock.** *Biophys J* 2008, **94**(4):1221–32.

[4] Hong CI, Ruoff P, Loros JJ, Dunlap JC: **Closing the circadian negative feedback loop: FRQ-dependent clearance of WC-1 from the nucleus.** *Genes Dev* 2008, **22**(22):3196–3204.

[5] Froehlich AC, Liu Y, Loros JJ, Dunlap JC: **White collar-1, a circadian blue light photoreceptor, binding to the frequency promoter.** *Science* 2002, **297**(5582):815–9.

[6] Crosthwaite SK, Loros JJ, Dunlap JC: **Light-induced resetting of a circadian clock is mediated by a rapid increase in frequency transcript.** *Cell* 1995, **81**(7):1003–12.

[7] Tan Y, Dragovic Z, Roenneberg T, Merrow M: **Entrainment dissociates transcription and translation of a circadian clock gene in Neurospora.** *Curr Biol* 2004, **14**(5):433–8.

[8] Linden H, Macino G: **White collar 2, a partner in blue-light signal transduction, controlling expression of light-regulated genes in Neurospora crassa.** *EMBO J* 1997, **16**:98–109.

[9] MacDonald N: *Biological Delay Systems: Linear Stability Theory*. Cambridge University Press; 1989.

[10] Locke JCW, Millar AJ, Turner MS: **Modelling genetic networks with noisy and varied experimental data: the circadian clock in Arabidopsis thaliana.** *J Theor Biol* 2005, **234**(3):383–93.

[11] Schafmeier T, Haase A, Káldi K, Scholz J, Fuchs M, Brunner M: **Transcriptional feedback of Neurospora circadian clock gene by phosphorylation-dependent inactivation of its transcription factor.** *Cell* 2005, **122**(2):235–46.

[12] Bratley P, Fox BL: **ALGORITHM 659: Implementing Sobol's quasirandom sequence generator**. *ACM Trans Math Softw* 1988, **14**:88–100.

[13] Press WH, Teukolsky SA, Vetterling WT, Flannery BP: *Numerical Recipes in C: The Art of Scientific Computing*. Cambridge University Press; 1996.

[14] Kirkpatrick S, Gelatt CD, Vecchi MP: **Optimization by simulated annealing.** *Science* 1983, **220**:671–680.

[15] Rand DA, Shulgin BV, Salazar D, Millar AJ: **Design principles underlying circadian clocks.** *J R Soc Interface* 2004, **1**:119–130.

[16] Rand DA, Shulgin BV, Salazar JD, Millar AJ: **Uncovering the design principles of circadian clocks: mathematical analysis of flexibility and evolutionary goals**. *J Theor Biol* 2006, **238**(3):616–635.

Supplementary Figures

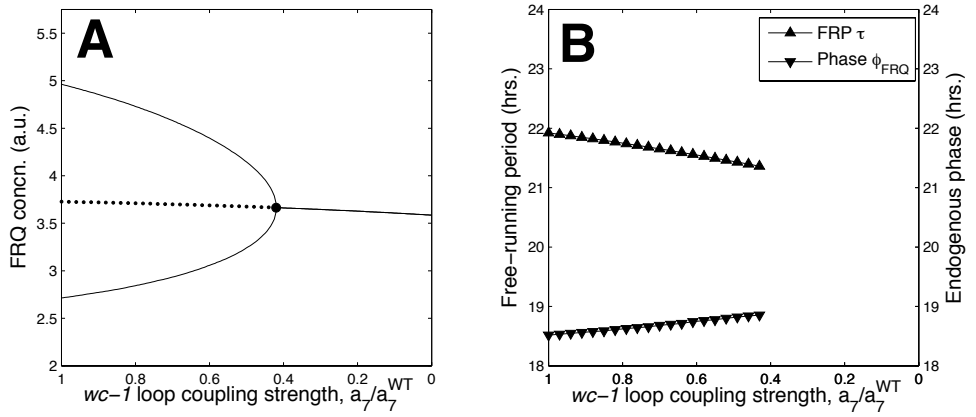

Figure S1: **A**. Bifurcation diagram showing the loss of rhythmicity in the simulated free-running (DD) system as the relative coupling strength a_7/a_7^{WT} of the *wc-1* loop is reduced (the parameter a_7 determines the rate at which FRQ protein upregulates WC-1 production, with a_7^{WT} indicating the WT value). For each coupling strength value on the x-axis, the corresponding values on the y-axis denote minimum and maximum FRQ levels. Solid lines denote stable attractors and broken lines unstable attractors. The solid circle indicates a supercritical Hopf bifurcation at which the attractor changes from a limit cycle (corresponding to rhythmicity) to a fixed point (corresponding to arrhythmicity). **B.** Corresponding variations in free-running period τ and the falling phase ϕ_{FRQ} of FRQ protein. ϕ_{FRQ} is calculated relative to the FRQ minimum, taken as CT 0.

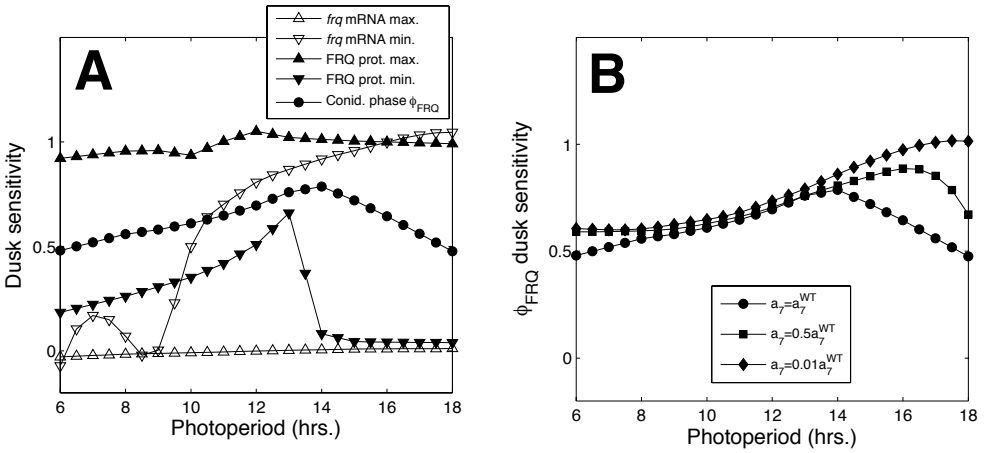

Figure S2: **A**. Variations in dusk sensitivity with photoperiod P for the phase measures plotted in Figure 4 of the main paper. Conidiation phase ϕ_{FRQ} has an intermediate sensitivity across the photoperiod range, indicating systematic entrainment (the higher sensitivities observed close to $P = 14$ correspond to the inflexion of the phase-photoperiod profile in Figure 4A). **B**. The effect of removing the *wc-1* loop on the dusk sensitivity-photoperiod profile of ϕ_{FRQ}. Note the pronounced increase in sensitivity for larger P values as the relative coupling strength a_7/a_7^{WT} is decreased.

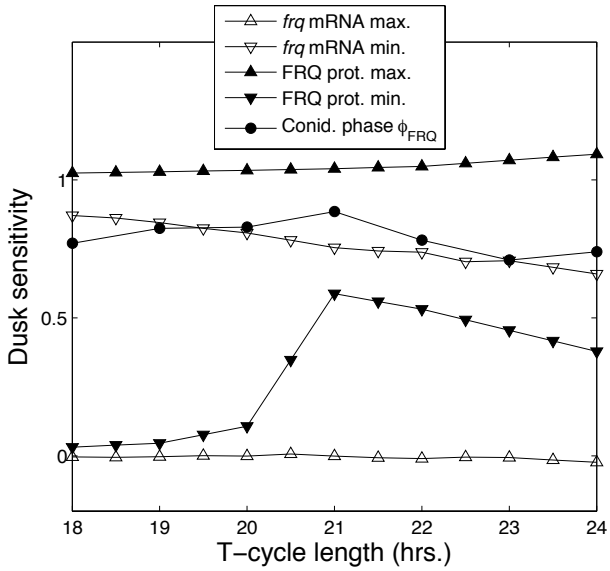

Figure S3: Dependence of the dusk sensitivities plotted in Figure 5 on T-cycle length. Conidiation phase ϕ_{FRQ} has a high sensitivity across the range shown, indicating a dusk-driven response.

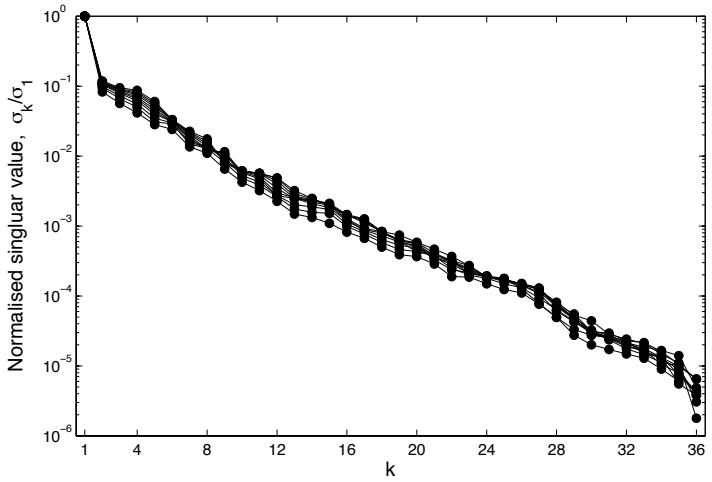

Figure S4: Normalised singular value spectra $\{\sigma_k/\sigma_1\}$ corresponding to each of the relative flexibility computations $F_\gamma\left(a_7|a_7^{WT}\right)$ plotted in Figure 7A. For all *wc-1* loop coupling strengths, the leading singular value σ_1 is larger than the others by an order of magnitude, showing that the decrease in flexibility with coupling occurs primarily along the first principal component of the entrained limit cycle.

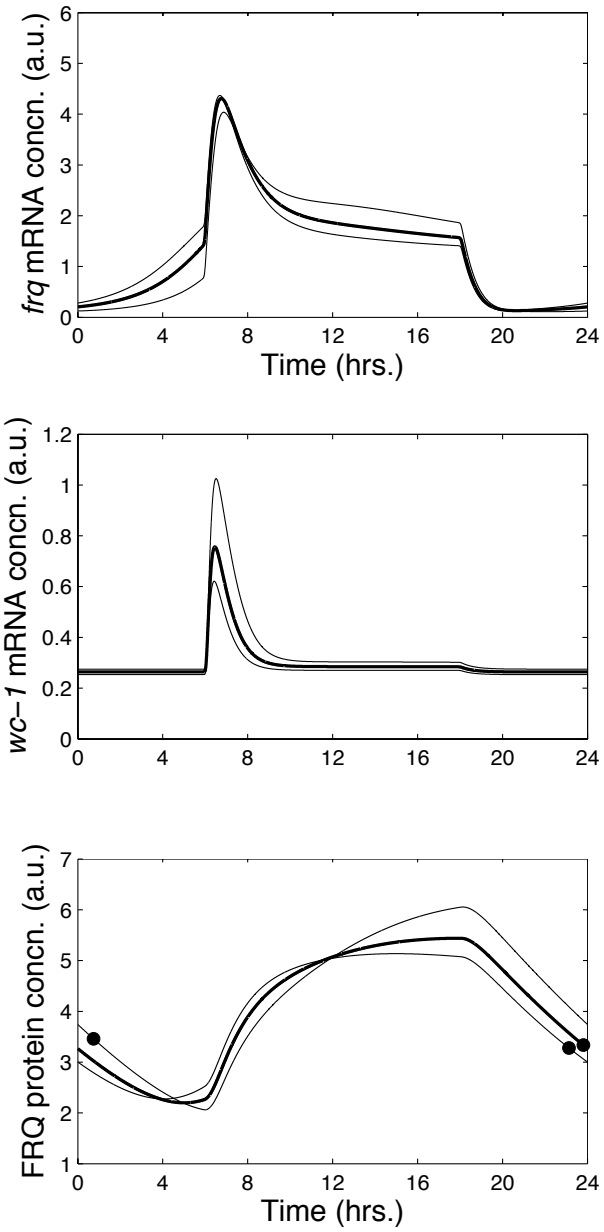

Figure S5: The effect of perturbing the WT solution of the model (thick solid lines) in the direction of the first principle component vector u_1 of the entrained limit cycle γ. Perturbed solutions (thin solid lines) were computed for proportional parameter variations of $\pm 2\%$ (that is for parameters $k_i = k_i^{WT}\,(1 \pm 0.02 v_{i1})$, where k_i^{WT} are the WT parameters and $v_1 = (v_{i1})$ is the right singular vector associated with u_1). Solid circles represent FRQ-dependent conidiation phase ϕ_{FRQ}. Note the greater flexibility in the phase of FRQ protein compared to that of *frq* and *wc-1* mRNA, consistent with the phase-amplitude sensitivity analysis shown in Figure 8A.

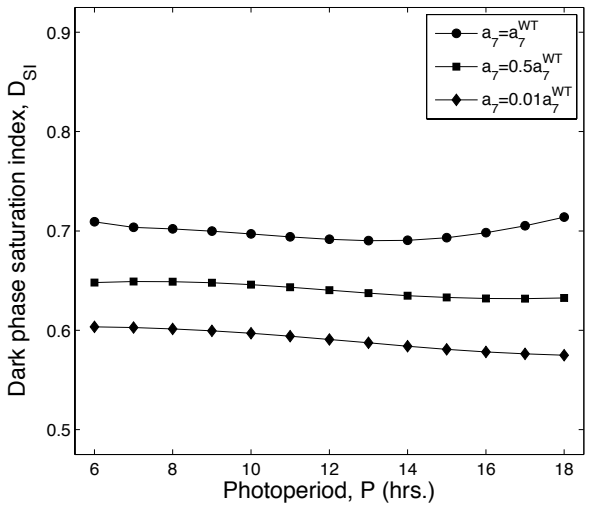

Figure S6: The effect of decreasing positive feedback strength a_7 on the FRQ degradation saturation index D_{SI} for different photoperiods P. D_{SI} is defined by $D_{SI} = \frac{1}{24-P}\int_{t_{DUSK}}^{t_{DUSK}+24-P} \frac{P_F(t)}{P_F(t)+b_6}dt$. Values of the measure closer to 1 denote a near-constant rate of FRQ loss during the night, resulting in FRQ profiles that decrease linearly with time. Note that reducing a_7 uniformly decreases D_{SI} across photoperiods, providing the system with a simple mechanism for tuning the level of saturation.